

Pathways to quiescence: SHARDS view on the Star Formation Histories of massive quiescent galaxies at $1.0 < z < 1.5$

Helena Domínguez Sánchez ^{1*}, Pablo G. Pérez-González¹, Pilar Esquej¹,
 M. Carmen Eliche-Moral¹, Guillermo Barro², Antonio Cava³, Belén Alcalde Pampliega¹,
 Nicolás Cardiel^{1,4}, Almudena Alonso Herrero⁴, Antonio Hernán Caballero⁴,
 Javier Cenarro⁵, Stéphane Charlot⁶, Gustavo Bruzual⁷

¹ Departamento de Astrofísica, Facultad de CC. Físicas, Universidad Complutense de Madrid, E-28040 Madrid, Spain

² University of California, 1156 High Street, Santa Cruz, CA 95064

³ Observatoire de Genève, Université de Genève, 51 Ch. des Maillettes, 1290 Versoix, Switzerland

⁴ Instituto de Física de Cantabria, CSIC-UC, 39005 Santander, Spain

⁵ Centro de Estudios de Física del Cosmos de Aragón, Plaza San Juan 1, 44001, Teruel, Spain

⁶ UPMC-CNRS, UMR7095, Institut d'Astrophysique de Paris, F-75014 Paris, France

⁷ Centro de Radioastronomía y Astrofísica, UNAM, Campus Morelia, México

Accepted. Received ; in original form

ABSTRACT

We present Star Formation Histories (SFHs) for a sample of 104 massive ($M > 10^{10} M_{\odot}$) quiescent galaxies (MQGs) at $z = 1.0$ – 1.5 . These SFHs have been inferred from the analysis of rest-frame ultraviolet/optical spectro-photometric data from the SHARDS and HST/WFC3 G102 and G141 surveys of the GOODS-N field, jointly with ancillary broad-band observations covering the UV-to-FIR spectral range. The sample of MQGs has been constructed on the basis of the rest-frame UVJ colors and specific star formation rates ($sSFR = SFR/mass$). The Spectral Energy Distributions (SEDs) of each galaxy have been compared to models assuming an exponentially declining SFH with 4 free parameters: age, star formation timescale, metallicity, and dust attenuation. The SED-fitting method includes a Monte Carlo algorithm to characterize in detail the uncertainties and the inherent degeneracies in this kind of study. Taking advantage of the SHARDS data resolution, we are able to break these degeneracies by measuring absorption indices such as Mg_{UV} and D4000. The population of MQGs at $z = 1.0$ – 1.5 shows a duality in their properties. Most of the sample ($\sim 85\%$) presents relatively young mass-weighted ages $\overline{t_M} < 2$ Gyr, short star formation timescales $\langle \tau \rangle \sim 60$ – 200 Myr and their average mass is $\log(M/M_{\odot}) \sim 10.5$. The evolution of these mature galaxies from $z \sim 1$ to $z = 0$ is consistent with being passive, but accompanied with a stellar mass increase (not affecting the mean ages). There is also an older population of galaxies ($\sim 15\%$ of the sample) with $\overline{t_M} = 2$ – 4 Gyr, larger star formation timescales $\langle \tau \rangle \sim 400$ Myr, and more massive $\log(M/M_{\odot}) = 10.8$. The number density of this sub-population of senior galaxies is consistent with that found for massive quiescent galaxies at $z \sim 2$, implying that these galaxies do not restart their star formation activity once they are quenched. We find that the derived SFHs for our MQGs are consistent with the slope and the location of the Main Sequence of star-forming galaxies (MS) at $z > 1.5$, when our galaxies were 0.5 – 1.0 Gyr old. According to the derived SFH, all of the MQGs experienced a Luminous Infrared Galaxy (LIRG) phase during typically ~ 500 Myr and roughly half of them went through ULIRG phase for ~ 100 Myr. Attending to the SFHs of MQGs at $1 < z < 1.5$, we find that the build-up of the red sequence is continuous at least down to $z \sim 1$, and only below that redshift (in the last 6 Gyr), the evolution of massive galaxies is dominated by quiescence.

Key words: galaxies: formation; galaxies: evolution; galaxies: high-redshift; galaxies: stellar content

1 INTRODUCTION

In the current paradigm of cosmic evolution, galaxies grow their mass by accreting gas from the cosmic web (e.g. Tacconi et al. 2010) and transforming it into stars. A tight relation between mass and SFR exists for normal star-forming galaxies, known as the main sequence (MS; e.g. Noeske et al. 2007; Elbaz et al. 2007; Rodighiero et al. 2010). Galaxies grow in mass within or above this main sequence until, eventually, the exhaustion of gas or some feedback mechanism halt the star formation. At this time, galaxies reach a quiescence state. The mass evolution of the quiescent population is then dominated by (dry) mergers of already assembled (smaller or similar in mass) galaxies. Λ CDM theory requires that more massive halos generally assemble later than less massive ones. However, over the past few decades there have been a series of observational results indicating that many processes, such as star formation, occur earlier in the most massive and luminous galaxies than in less massive galaxies, in an scenario called *downsizing* (Cowie et al. 1996; Madau et al. 1996; Cimatti et al. 2006; Bundy et al. 2007; Pérez-González et al. 2008; Ilbert et al. 2010).

Concentrating in the evolution of the most massive galaxies along the lifetime of the Universe, we now know that many of such systems were already assembled at high redshifts (Pérez-González et al. 2008; Marchesini et al. 2009; Ilbert et al. 2013; Muzzin et al. 2013; Tomczak et al. 2014; Grazian et al. 2015). Moreover, a significant fraction of high- z massive galaxies were not forming stars anymore and evolving passively (Cimatti et al. 2004; Daddi et al. 2005; Papovich et al. 2006; Fontana et al. 2009; Santini et al. 2009; Domínguez Sánchez et al. 2011; Ilbert et al. 2013), i.e., they were MQGs. The number densities of MQGs at intermediate redshifts are in disagreement with semi-analytical models (e.g. Pozzetti et al. 2010; Ilbert et al. 2013; Muzzin et al. 2013). Besides, the observed MQGs at high- z are found to be much more compact than their local analogues, implying a strong mass-size evolution with cosmic time (e.g. Trujillo et al. 2006; Buitrago et al. 2008; van Dokkum et al. 2008; Barro et al. 2014).

Understanding the formation mechanisms of this population of MQGs is fundamental to improve our picture of galaxy evolution. In particular, having an accurate description of the Star Formation Histories (SFHs) of these galaxies is crucial to have a good estimation of the times needed by physical processes to ignite star formation and then quench it in massive galaxies. However, up to date, there are few results on the individual properties and SFH of MQGs at high- z , mostly because estimating SFHs is very hard with the data we typically have at hand.

Quiescent galaxies at high- z are difficult to observe in the optical bands as their emission in the rest-frame UV is weak, due to the absence of high energy processes such as star formation, and dominated by absorption features (e.g., Daddi et al. 2005; Cimatti et al. 2008; van Dokkum et al. 2011). Indeed, these galaxies show no emission lines and absorption features related to an old and passively evolved stellar population. However, spectroscopic observations are time consuming and are therefore limited to a small number of galaxies or to the analysis of stacked spectra (Bedregal et al. 2013; Whitaker et al. 2013; Belli et al. 2015).

Thanks to the arrival of deep and wide multi-wavelength photometric surveys such as COSMOS (Lilly et al. 2007), ULTRA-VISTA, (McCracken et al. 2012) or CANDELS (Grogin et al. 2011; Koekemoer et al. 2011), the mass functions and number densities of quiescent galaxies have been studied up to $z \sim 3-4$. But the spectral resolution of photometric data is not enough to study in

detail the stellar population properties. The main reason is the presence of strong degeneracies in the analysis of their spectral energy distribution (SEDs) using stellar population synthesis. These degeneracies are mainly related to the similar effect of different levels of dust attenuation, age, and metallicity in very low spectral resolution data ($R \sim 7$, typical of broad-band studies). This indeed complicates the accurate determination high- z galaxy properties based on SED-fitting and the only reliable parameter obtained in this kind of studies is the stellar mass (Elsner et al. 2008; Santini et al. 2015).

In order to break the typical degeneracies inherent to any study of stellar populations in distant galaxies, we need data whose spectral resolution is higher than broad-band photometry (Pacifiçi et al. 2013). There are spectral features which help to break these degeneracies. For example, the Mg_{UV} index probes several absorption lines (e.g., MgI $\lambda 2852$, MgII $\lambda \lambda 2796, 2804$, $\lambda \lambda$ FeII 2600, 2606) and has been shown to be extremely reliable to identify galaxies dominated by evolved stars. Moreover, these absorption lines can be used to easily distinguish the SED of a quiescent massive galaxy from the featureless spectrum of a dusty starburst (Daddi et al. 2005). The break in the stellar continuum at 4000 Å is also a good age indicator (Bruzual 1983; Balogh et al. 1999; Kauffmann et al. 2003). It arises because of the accumulation of a large number of spectral lines in a narrow wavelength region. Given the dependence of D4000 on stellar atmospheric parameters (Gorgas et al. 1999), it is very prominent for galaxies older than ~ 1 Gyr. The strength of the 4000 Å break for a single stellar population increases with its age and depends weakly on the metallicity at low ages ≤ 1 Gyr (Hernán-Caballero et al. 2013). The Mg_{UV} and D4000 indices have been successfully used in the past to obtain redshifts and ages of stellar populations in massive galaxies at high- z (Saracco et al. 2005; Kriek et al. 2011; Ferreras et al. 2012).

In this work, we take advantage of the spectro-photometric resolution of the Survey for High- z Absorption Red and Dead Sources survey (SHARDS, Pérez-González et al. 2013) to obtain robust estimations of the SFH of MQGs at high redshift. SHARDS is an ultra-deep optical survey of the GOODS-N field covering the wavelength range between 500 and 950 nm with 25 contiguous medium-band filters, providing a spectral resolution $R \sim 50$. We combine the SHARDS observations with spectroscopic data from the HST WFC3 G102 and G141 grisms covering 0.9-1.6 μ m, as well as with multi-wavelength ancillary data from from UV to FIR extracted from the Rainbow database (Pérez-González et al. 2008; Barro et al. 2011). We, therefore, count with data with a spectral resolution $R \sim 50$ or better from 500 nm to 1.6 μ m (jointly with broad-band photometry), a significant improvement from previous works on the subject. We perform a SED-fitting to the whole wavelength range (up to the IRAC bands) using delayed exponentially declining stellar population models. Thanks to the unique photometric dataset and spectral coverage of this work, we are able to account for the degeneracies and study in detail and individually the SFH (masses, SFR, ages, star formation timescales, dust attenuations and metallicities) of a sample of MQGs at $z = 1.0-1.5$, discussing the implications for the early mass assembly of galaxies.

The structure of this paper is as follows: In Sect. 2, we present the data and the sample selection. In Sect. 3, we explain the SED-fitting method and the procedure to characterize the degeneracies inherent to stellar population analysis. In Sect. 4, we analyze the derived properties and the time-evolution of our sample of MQGs on the basis of their SFHs. Finally, in Sect. 5, we summarize our conclusions.

Throughout this work, we standardize to a $(h, \Omega_M, \Omega_\Lambda) = (0.7, 0.3, 0.7)$ Wilkinson Microwave Anisotropy Probe (WMAP)

concordance cosmology (Spergel et al. 2003), AB magnitudes, (Oke & Gunn 1983), a Kroupa 2001 IMF (integrated from 0.1 – 100 M_{\odot}) and Bruzual & Charlot (2003) (BC03, hereafter) stellar population synthesis models.

2 DATA AND SAMPLE SELECTION

In this work, we analyze a sample of massive ($M > 10^{10} M_{\odot}$) quiescent galaxies (MQGs) at $1.0 < z < 1.5$ selected with two different criteria: using their rest-frame UVJ colors, and also based on their specific Star Formation Rates (sSFR). In the following subsections, we describe the datasets gathered for this work, as well as the details about the selection criteria.

2.1 Data

Our sample was selected in the 130 arcmin² covered by the Survey for High- z Absorption Red and Dead Sources survey (SHARDS, Pérez-González et al. 2013) survey in the GOODS-N region. SHARDS is an ESO/GTC Large Program carried out with the OSIRIS instrument on the 10.4 m Gran Telescopio Canarias (GTC). It consists of an ultra-deep optical spectro-photometric survey of the GOODS-N field at wavelengths between 500 and 950 nm using 25 contiguous medium-band filters which provide a spectral resolution $R \sim 50$. The data reach an AB magnitude of 26.5 (at least at a 3σ level) with sub-arcsec seeing in each one of the 25 bands. More details about the reduction and calibration of the SHARDS data can be found in Pérez-González et al. (2013).

For this paper, we complement the SHARDS data with the G102 and G141 grism observations of the GOODS-N field carried out with the HST/WFC3 instrument. The G102 spectroscopic program (PI: Barro) covers the spectral region between 800 and 1150 nm with $R \sim 210$ and a 5σ magnitude limit of 21.5 mag in the F140W band. The G141 data (PI: Weiner) covers from 1100 to 1700 nm with $R \sim 130$ and a 5σ limit of 21.5 mag in the F160W band. The WFC3 grism spectroscopic data were reduced using the aXe software version 2.3. Based on the 2D spectra provided by aXe, we extracted 1D spectra for each galaxy in our sample using the effective radius as the extraction width. We visually inspected each spectrum, adjusting the extraction parameters (aperture width and spectral range), to avoid contamination from nearby sources. We refer the reader to Esquej et al. (in prep.) for a detailed description of the reduction and extraction of WFC3 grism data.

Jointly with the SHARDS and WFC3 grism data, we also use in our analysis the ancillary multi-wavelength catalog and advanced products in the GOODS-N field presented in Pérez-González et al. (2008) and compiled in the Rainbow Cosmological Surveys Database¹ (see also Pérez-González et al. 2008; Barro et al. 2011). This dataset includes observations from X-rays to the Far-IR and radio bands, as well as spectroscopic data in the GOODS-N field from the literature. In Pérez-González et al. (2008), we presented a merged photometric catalog including broad-band data for a stellar mass selected sample based on ultra-deep IRAC observations. For this work, we have merged this catalog with the SHARDS and WFC3 grism datasets. Using the full SED, we carried out a stellar population modeling which provided accurate photometric redshifts, stellar masses, SFRs, and

rest-frame synthetic colors for $\sim 26,000$ stellar mass selected galaxies in the region of the GOODS-North field covered by SHARDS.

Concerning photometric redshifts, the ultra-deep medium band SHARDS data allowed us to obtain high quality photometric redshifts for all sources, which will be presented in Barro et al. (2015, in preparation). The median $|\Delta z|/(1+z)$ is 0.0067 for the 2650 sources with $I < 25$ and spectroscopic redshifts (see also Ferreras et al. 2014).

As described in Pérez-González et al. (2008), the parent sample used in this paper, selected with ultra-deep IRAC imaging as a proxy for stellar mass, is complete for galaxies with $M_{\star} \geq 10^{9.5} M_{\odot}$ up to $z = 1.5$ and a maximally old stellar population. The IRAC selection is biased against younger galaxies with large attenuations and masses $M < 10^{10} M_{\odot}$, so we impose this mass limit in the definition of our final sample of MQGs.

Synthetic rest-frame colors were estimated for all galaxies in the parent sample by convolving the best-fitting stellar population models with transmission curves for standard filters. In this paper, we will use the Johnson U and V filters, as well as the 2MASS J -band filter to construct a UVJ diagram and select quiescent galaxies. We note that the actual transmission curves for which we estimated UVJ rest-frame absolute magnitudes were tweaked to match the color distribution in the UVJ diagrams presented in Whitaker et al. (2011). This is the paper we used for the quiescence definition.

Finally, in order to select quiescent galaxies for this paper, SFRs were estimated for all galaxies in the parent sample based on either mid- and far-IR data from *Spitzer* and *Herschel*, or from UV luminosities. In the case of IR emitters, GOODS-N has been observed with the deepest MIPS data in the sky, with a 5σ limit of 30 μJy (Pérez-González et al. 2005), and also very deep PACS and SPIRE images, with 5σ limits of 1.7 mJy and 9 mJy at 100 μm and 250 μm , respectively. These limits (the deepest being MIPS 24 μm data) correspond roughly to 5-10 $M_{\odot} \text{ yr}^{-1}$ for galaxies at $1.0 < z < 1.5$ (see Pérez-González et al. 2005 and Elbaz et al. 2011). The SFR for IR detected galaxies was derived following Kennicutt (1998, see also Bell et al. 2005) normalized to a Kroupa IMF:

$$\text{SFR}_{UV+IR} = 1.15 \times 10^{-10} (L_{IR} + 3.3 \times L_{280}) [M_{\odot} \text{ yr}^{-1}] \quad (1)$$

where L_{280} is the luminosity at rest-frame 280 nm in erg s^{-1} .

In order to estimate SFRs for galaxies not detected in the mid- or far-IR, we used UV luminosities at rest-frame 280 nm. These luminosities were converted into SFRs by applying Kennicutt (1998) equation normalized to a Kroupa IMF:

$$\text{SFR}_{UV} = 0.98 \times 10^{-28} \times L_{UV} [M_{\odot} \text{ yr}^{-1}] \quad (2)$$

The UV-based SFRs were corrected for attenuation following a recipe based on the UV/IR- β relation (IRX- β). The UV slope β for each galaxy was measured from the SEDs described above, interpolating in the best fitting models between 150 and 300 nm. In order to convert these slopes to an attenuation, we used the comparison between the observed UV and IR-based SFRs for galaxies detected by MIPS (Figure 1). Typical attenuation recipes based on the UV slope are derived for galaxies with high levels of star formation (Meurer et al. 1999; Takeuchi et al. 2012), which are dustier than relatively quiescent galaxies. Quiescent galaxies have systematically lower ratio of total far-infrared to ultraviolet luminosity than starburst galaxies (Kong et al. 2004). Given that in this paper we are interested in galaxies with very low levels of star formation, and in order to avoid an over-correction for dust attenuation, we

¹ <http://rainbowx.fis.ucm.es>

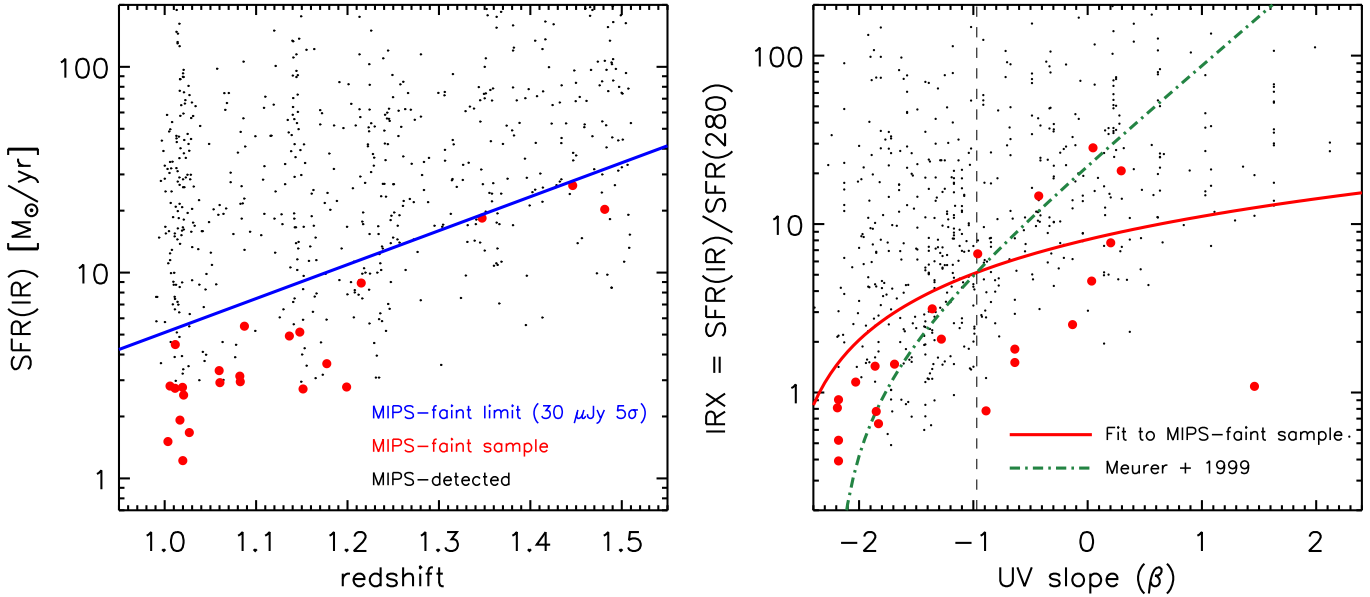


Figure 1. SFR(IR) vs. redshift (*left panel*) and IRX- β relation (*right panel*) for our sample of massive ($M > 10^{10} M_{\odot}$) galaxies at $1.0 < z < 1.5$ detected by MIPS at $24 \mu\text{m}$. The red points (23 galaxies) are selected faint IR emitters, i.e., galaxies with an IR emission lower than the MIPS24 5σ limit ($30 \mu\text{Jy}$). The corresponding SFR(IR) for that detection limits is shown with a blue line. To avoid biasing the fits in the IRX- β plot, we randomly chose a subsample of faint IR emitters homogeneously covering the whole range of UV slopes β . We fit the IRX- β (linear) relation for the faint IR emitters (red line) to obtain a β -based dust attenuation for the population of galaxies with low levels of star formation. The green line is the IRX- β fit from Meurer et al. (1999), based on the analysis of regular star-forming galaxies and starbursts. Note that the dust attenuation correction at high β values is much smaller for the IR-faint sample compared to IR-bright galaxies.

derived a UV/IR- β relation for faint-IR emitters, i.e., those galaxies for which their IR detection is below the 5σ IR detection limit at that redshift. In comparison with bright-IR galaxies or the local starbursts studied in, e.g., Meurer et al. (1999), this sub-sample should present attenuation properties which are closer to the MQGs that we want to study. The procedure is outlined in Figure 1, where we show SFR(IR) versus redshift, and the IRX- β relation for the galaxies at $1.0 < z < 1.5$ detected by MIPS. We highlight the galaxies which are faint-IR emitters, for which we derive the following IRX- β relation:

$$\text{IRX} \equiv \frac{\text{SFR(IR)}}{\text{SFR(280)}} = 8.09 + 3.02 \times \beta \quad (3)$$

We apply the Meurer et al. (1999) IRX- β relation for β values lower than the cross-point ($\beta = -0.97$) with Meurer et al. (1999) and Eq. 3 for higher β values.

2.2 Selection of quiescent galaxies

To construct a complete and uncontaminated sample of MQGs at $z=1.0-1.5$, we used two complementary methods: a *UVJ* diagram and sSFRs. We only consider galaxies with $M > 10^{10} M_{\odot}$, for which our survey is complete within the considered redshift range.

2.2.1 Quiescence criterion based on the *UVJ* color-color diagram

There are 410 galaxies with $M > 10^{10} M_{\odot}$ at $z=1.0-1.5$ in the Rainbow catalog of the GOODS-N field. The median stellar mass and sSFR of this sample are $M \sim 10^{10.4} M_{\odot}$ and $\text{sSFR} \sim 0.6 \text{ Gyr}^{-1}$. In Figure 2, we plot a *UVJ* diagram including all these galaxies.

Whitaker et al. (2011) defines the following as the region in the *UVJ* diagram where quiescent galaxies are located:

$$\begin{aligned} (U - V) &> 1.3 \\ (V - J) &< 1.6 \\ (U - V) &> 0.875 \times (V - J) + 0.6 \end{aligned} \quad (4)$$

We find 87 galaxies with $M > 10^{10} M_{\odot}$ in the quiescent region of the *UVJ* diagram. Out of these, 25 % are detected by MIPS, implying either some level of (obscured) star formation or nuclear activity. We eliminate them from this *UVJ*-selected sample of quiescent galaxies. The sample of MQGs selected with the *UVJ* diagram and no IR detection is composed by 65 galaxies. The median and quartile stellar mass for this sample is $\log(M/M_{\odot}) = 10.7_{10.4}^{10.9}$, they lie at $z = 1.17_{1.04}^{1.26}$, and have $\text{sSFR} = 0.07_{0.03}^{0.10} \text{ Gyr}^{-1}$. We will refer to the galaxies selected in this way as “*UVJ*-selected” galaxies and we will discuss their properties in Section 4.2.

2.2.2 Quiescence criterion based on sSFR values

We complement the selection based on the *UVJ* diagram with a cut in sSFR. We arbitrarily choose $\text{sSFR} < 0.2 \text{ Gyr}^{-1}$ as our limit for quiescence, given that imposing this value we are able to recover virtually all the sources identified as dead by the *UVJ* criterion (right panel of Figure 2).

We find 102 galaxies with $M > 10^{10} M_{\odot}$ and $\text{sSFR} < 0.2 \text{ Gyr}^{-1}$. All galaxies identified as quiescent in the *UVJ* diagram have $\text{sSFR} < 0.2 \text{ Gyr}^{-1}$, except 2. With a maximum $\text{sSFR} < 0.38 \text{ Gyr}^{-1}$, these 2 galaxies have relatively young stellar populations ($t < 0.8 \text{ Gyr}$) and short star formation timescales ($\tau < 60 \text{ Myr}$), as we discuss in Section 3. Note that among the sSFR-based sample we have 22 IR emitters (21% of the sSFR-selected sample). These

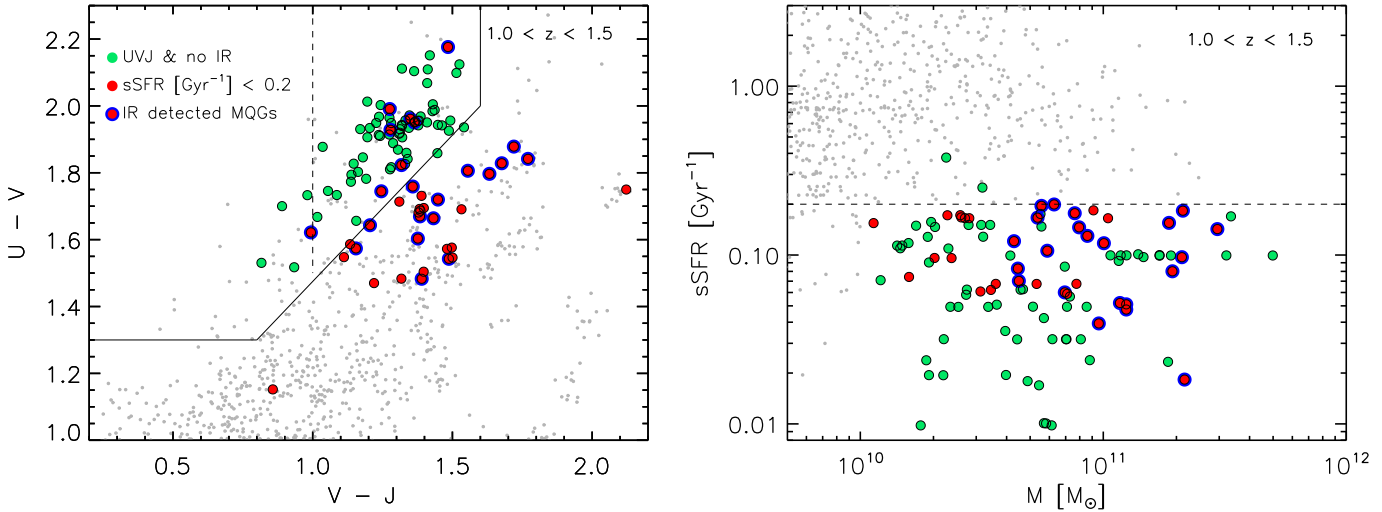


Figure 2. Plots showing the criteria to select the MQG sample. *Left panel:* UVJ diagram for galaxies at $z=1.0-1.5$ (gray dots). The final sample of MQGs (104 objects) are marked with black empty circles. The continuous line delimits the region where quiescent galaxies should be located, according to Whitaker et al. (2011). The dashed line splits the previous region in two, with post-starburst galaxies located on the left. The UVJ -selected galaxies are colored in green, and the sSFR-selected in red. The large blue circles mark IR detected galaxies (only for galaxies with $sSFR < 0.2 \text{ Gyr}^{-1}$). *Right panel:* sSFR versus stellar mass, color coded as in the left panel. The dashed line represents our limit to consider a galaxy as quiescent ($sSFR < 0.2 \text{ Gyr}^{-1}$).

galaxies must have some (residual) star formation or nuclear activity, but their mass is large enough ($\log(M/M_{\odot}) > 10.4$) to present sSFRs values comparable to dead galaxies undetected in the IR. The median and quartiles for the stellar mass distribution of our sample is $\log(M/M_{\odot}) = 10.8^{11.0}_{10.5} M_{\odot}$, they lie at $z = 1.15^{1.24}_{1.02}$, and have $sSFR = 0.07^{0.16}_{0.10} \text{ Gyr}^{-1}$. With this sSFR criterion, we recover 8 galaxies located in the UVJ quiescent region which were discarded in the color-color selection because of their IR detection. However, they have low enough sSFR values ($< 0.18 \text{ Gyr}^{-1}$) to be selected in our MQG sample. We will refer to galaxies selected in this way as “sSFR-selected” galaxies, and we will discuss their properties in Section 4.2. Note that this is a complementary sample to the UVJ -selected, i.e., they are galaxies with $sSFR < 0.2 \text{ Gyr}^{-1}$ but excluding the 65 previously selected with the UVJ criteria, resulting in 39 additional galaxies.

Combining the UVJ and sSFR criteria, we arrive to a sample of MQGs with $M > 10^{10} M_{\odot}$ composed by 104 sources. The main properties of the sample divided by their selection criteria can be found in Table 3. In Figure 3 we show the postage stamps made with HST ACS/WFC3 for the final sample of MQGs selected in this work.

2.2.3 Statistical properties of the sample

The combined UVJ - and sSFR-selected sample of MQGs was refined by carrying out a detailed stellar population synthesis analysis of each galaxy. We constructed the most detailed SED possible for each galaxy combining the ultra-deep SHARDS data with the G102 and G141 spectro-photometric observations. This provides SEDs with up to 150 photometric points at a photo-spectral resolution from 500 nm to $1.6 \mu\text{m}$. Galaxies without G141 or G102 spectra have at least 30 photometric data points (see Sect. 2.2). This unique photometric dataset encompasses, within the whole observed redshift range, significant spectral features related to the age of the galaxies, such as the break at 4000 \AA , D4000, or the ultraviolet magnesium index, Mg_{UV} . Our final sample of MQGs at $z = 1.0 - 1.5$ consists of 104 galaxies, 65 UVJ -selected plus

39 sSFR-selected. There are 54 (52%) galaxies for which spectroscopic redshifts are available, and the photometric redshift quality for them is characterized by a median $|\Delta z|/(1+z) = 0.0047$. They are detected at 3σ in at least 13 SHARDS bands. Concerning the availability of grism data, 60% and 70% of the final sample have usable G102 and G141 spectra with typical $\text{SNR} \sim 11$. The rest have either severe contamination problems or are too faint for the grism observations. MQGs represent $\sim 25\%$ of the population of massive galaxies within the same redshift interval. They have median values $\log(M/M_{\odot}) = 10.7^{11.0}_{10.4} M_{\odot}$, $z = 1.17^{1.25}_{1.03}$, and $sSFR = 0.10^{0.15}_{0.05} \text{ Gyr}^{-1}$.

The fraction of quiescent galaxies in a mass-selected sample according to our analysis is in good agreement with the 28% reported by Muzzin et al. (2013) for a purely UVJ selected sample of quiescent galaxies with $\log(M/M_{\odot}) > 9.5$ at $z = 1.0 - 1.5$. The fraction of MQGs that we find is larger than the 13% of quiescent galaxies with $\log(M/M_{\odot}) > 9.6$ at $z = 1.1 - 1.5$ selected on the basis of their NUV, r^+ and J colors found by Ilbert et al. (2013). The fraction of very massive ($\log(M/M_{\odot}) > 10.85 M_{\odot}$) quiescent galaxies (selected on the basis of IR colors and $sSFR_{\text{SED}} < 0.01 \text{ Gyr}^{-1}$) derived in Fontana et al. (2009) at $z \sim 1.2$ is $\sim 40\%$, quite larger than the $\sim 25\%$ that we obtain with the same mass cut. We will further discuss our results about the properties of our sample of MQGs and compare them with the literature in Section 4.3.

3 METHODOLOGY TO DETERMINE THE STAR FORMATION HISTORIES OF MQGS

3.1 SED fitting

Our main goal in this paper is studying in detail the star formation histories (SFHs) of MQGs at $1.0 < z < 1.5$. For this purpose, we fit the observed photometry to stellar population synthesis models using the *synthesizer* fitting code described by Pérez-González et al. (2003, 2008). We use models with one burst of star formation characterized by a delayed exponentially declining SFH:

$$\text{SFR}(t) \propto t/\tau^2 \times e^{-t/\tau} \quad (5)$$

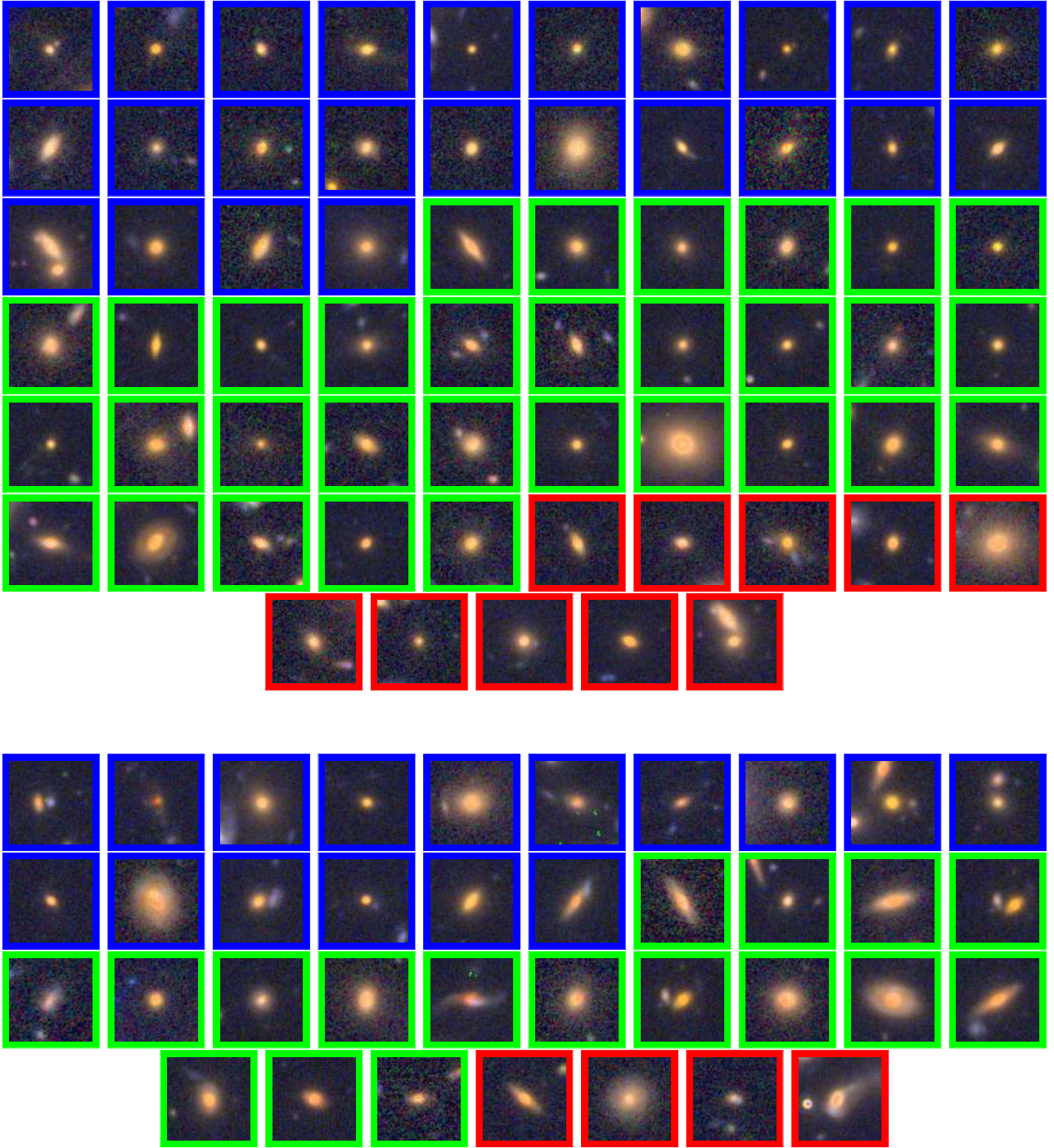


Figure 3. $5'' \times 5''$ postage stamps made with HST ACS/WFC3 for the 104 MQGs selected in this work (there are 2 galaxies missing because they are outside the WFC3 region). Galaxies in the upper panel are UVJ -selected, while galaxies in the lower panel are $sSFR$ -selected. In each panel, they are ranked (from left to right, top to bottom) by increasing mass-weighted age \overline{t}_M (see Sect. 4). Postage stamps for the 3 sub-samples of galaxies defined in the text based on mass-weighted ages are framed in blue (mature galaxies), green (intermediate), and red (senior galaxies).

The most common SFH parametrization used in the literature is an exponentially declining function. We, however, have chosen a more realistic parametrization with an initial increase in the star formation activity followed by an exponential decay, avoiding the nonphysical infinite derivative at time 0 in the pure exponentials. This parametrization is also closer to the SFHs predicted by galaxy evolution models (e.g. Pacifici et al. 2013; Barro et al. 2014).

We compare our SEDs with the BC03 stellar population li-

brary, assuming a Kroupa (2001) IMF, and the Calzetti et al. (2000) attenuation law. We allow 3 different metallicity values, $Z/Z_{\odot} = 0.4, 1.0$ and 2.5 , which correspond to values of sub-, solar and super-solar metallicity. Although it is commonly assumed in the literature that galaxies have solar metallicity, it is well known that galaxies may have different metal contents. For example, the mass-metallicity relation (Tremonti et al. 2004) points out that, at low redshift, more massive galaxies are more metallic. The metallic-

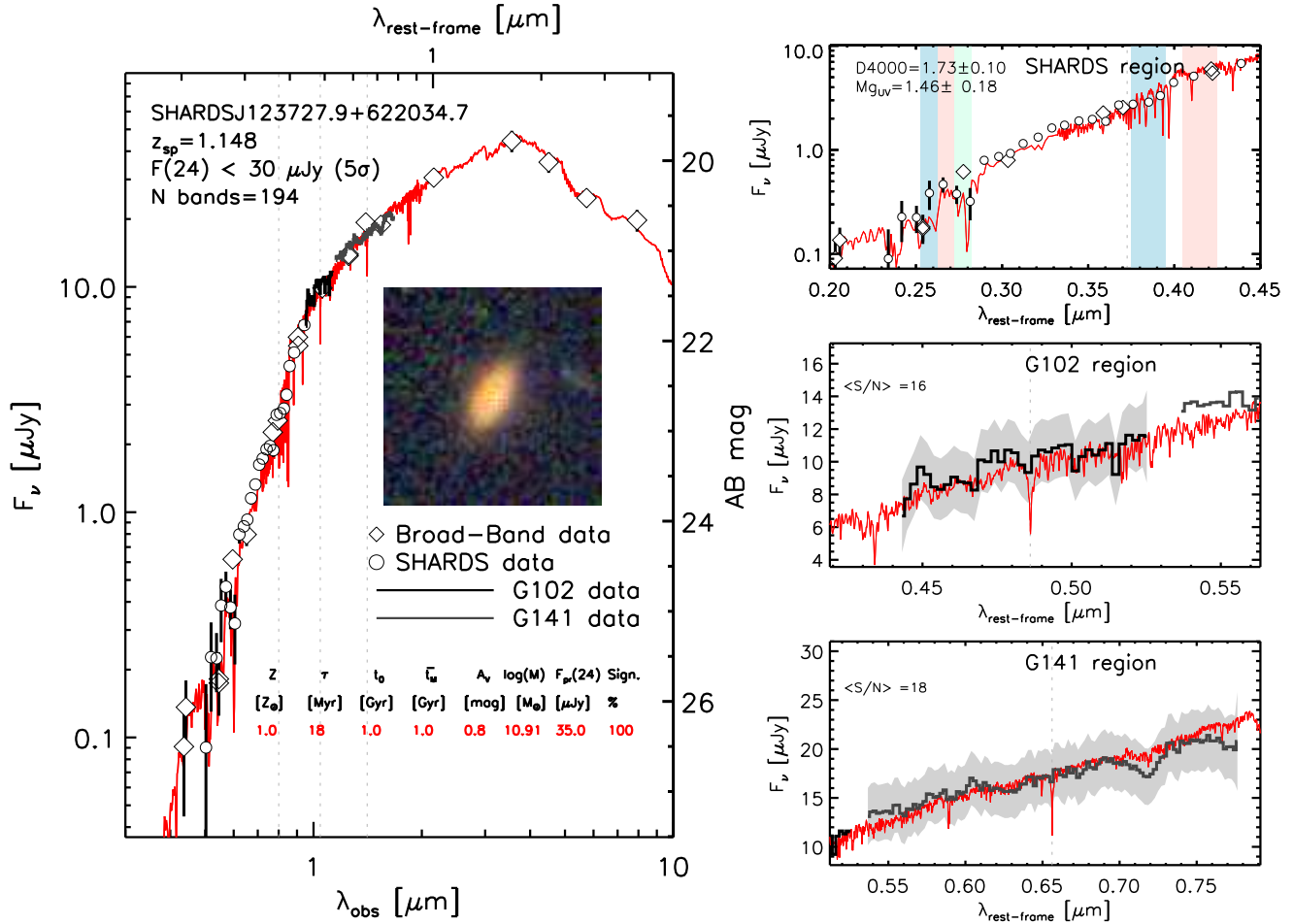


Figure 4. Example of SED-fitting for one of our MQGs, SHARDSJ123727.9+622034.7, a galaxy at $z=1.148$. In the left panel we show the SED-fitting to the whole dataset gathered for our work (194 data points). The white circles represent the SHARDS spectro-photometric data and the diamonds are broad-band data. The G102 and G141 spectra are plotted as black and dark grey lines and zoomed in the central and bottom right panels. We depict 3σ errors in all plots (and the average S/N in the grism spectrum plots). The vertical lines show the location of typical emission lines ($H\alpha$, $H\beta$ and $[\text{OII}]\lambda 3727$). We also show a $5'' \times 5''$ postage stamp made with HST ACS/WFC3 data. In the upper right panel, we show a zoom in the SHARDS region. The colored areas represent the bands used to determine the Mg_{UV} and D4000 indices, whose values are given in the legend. For this galaxy, only one stellar population model was compatible with the data after applying the method described in Section 3.2. The best-fitting parameters are shown in the legend, including metallicity, star formation timescale, age, mass-weighted age, dust attenuation, stellar mass, predicted $24 \mu\text{m}$ flux (see Sect. 3.3) and statistical significance of the solution.

ity also affects the shape of the SED, making galaxies look redder as we move to higher metallicities. Although the metallicities may take many more values, using only the 3 discrete values around solar metallicity given by the BC03 models is a sufficient approximation to see the effect of this parameter in our results.

Our stellar population synthesis code, *synthesizer*, performs a χ^2 minimization and returns the model which best fits the data. The age (t_0), timescale (τ), attenuation (A_v) and metallicity (Z) are set as the free parameters to fit. The ranges of free parameter values allowed in the fitting are given in Table 1. The stellar mass (M) of each galaxy is derived as the normalization of the best-fitting template to the median observed flux.

In the following sections, apart from the stellar population parameters mentioned above, we will also discuss mass-weighted ages (\bar{t}_M). The \bar{t}_M is defined as:

$$\bar{t}_M = \frac{\int_0^{t_0} \text{SFR}(t) \times t \, dt}{\int_0^{t_0} \text{SFR}(t) \, dt} = \frac{\int_0^{t_0} \text{SFR}(t) \times t \, dt}{M} \quad (6)$$

where t_0 is the best-fitting age, and M is the best-fitting mass.

An example of the SED fitting results is presented in Figure 4, where we show the fit to the whole wavelength interval, as well as zooms in the spectral regions covered by SHARDS, and the G102 and G141 grisms.

Our fitting code also includes an algorithm to estimate uncertainties in the derived parameters and study (and break when possible) the degeneracies typically present in SED-fitting studies. This algorithm involves a Montecarlo technique, and the use of direct measurements of spectral indices with the SHARDS and WFC3/grism spectro-photometric data (especially D4000 and Mg_{UV}), as well as the analysis of the mid- and far-IR fluxes and upper limits. We describe this algorithm in detail in the following subsection.

Parameter	range/values	units	step
age (t_0)	0.04 – 6.3	Gyr	0.1 dex
timescale (τ)	3 – 10000	Myr	0.1 dex
dust attenuation (A_v)	0 – 1.5	mag	0.1 mag
metallicity (Z)	0.4, 1.0, 2.5	Z/Z_\odot	discrete

Table 1. Free parameters (age, star formation timescale, dust attenuation and metallicity) and their allowed ranges used in the SED-fitting procedure.

3.2 Estimating uncertainties and analyzing degeneracies with a Montecarlo algorithm

We used a Montecarlo approach to estimate uncertainties in the stellar population properties and take into account the possible degeneracies of the SED-fitting technique. For each galaxy, we allowed the photometric data points to randomly vary following a Gaussian distribution with a width given by the photometric errors. In this way, we constructed 1000 modified SEDs for each object, and we then performed again the SED-fitting to the new photometric data. Therefore, for each galaxy we obtained 1000 different solutions and 1000 different set of parameters. This is fundamental to understand the degeneracies. In the SED-fitting procedure, the stellar population modeling code looks for best-fitting ages, timescales, metallicities, and dust attenuations in a grid of discrete values. In order to account for the discrete distribution of the fitting parameters probed by the minimization algorithm, we introduce Gaussian noise to the output parameters of each galaxy using a width equal to the step used for each fitted property (see Table 1).

Once we had 1000 SED-fitting solutions for a given galaxy, we looked for clusters of solutions in the τ - t_0 parameter space. We identified those clusters with a k-means method and a minimal separation of 0.2 dex between different solutions (i.e., the difference between the median cluster properties must be at least 0.2 dex in age and τ). Solutions which provide similar results are grouped as a single solution identified by a median value and a scatter in the multi-dimensional t_0 - τ - A_v - Z space. Using the full set of solutions for a given cluster, we calculate the values enclosing 68% of the data around the median. These are assumed to be the uncertainties of our estimations for each cluster of solutions. The typical relative uncertainties of the four free parameters in our analysis and the stellar mass are $\Delta\tau=30\%$, $\Delta t_0=25\%$, $\Delta A_v=0.15$ mag and $\Delta M=0.1$ dex. The metallicity uncertainties could not be determined because the allowed Z values are discrete.

Each cluster was assigned a statistical significance given by the fraction of solutions belonging to that cluster. The clusters represent the *significant* solutions of a galaxy taking into account the degeneracies in the determination of stellar properties from SED-fitting. Although we used the t_0 - τ plane to look for different solutions, we tested whether looking for clusters in the whole t_0 - τ - A_v - Z multi-dimensional space changed the results. Given that all the parameters are highly correlated, we found no difference between both approaches, i.e., a cluster analysis in one plane was able to robustly recover clusters in the 4-dimensional space.

In Figure 5, we show the SED-fitting results for one galaxy for which we find three clusters of solutions. The most significant (74% of solutions belong to this cluster) is a relatively young stellar population ($\overline{t_M} \sim 1.4$ Gyr) with a star formation timescale $\tau \sim 160$ Myr, moderate dust attenuation ($A_v=0.3$ mag), and super-solar metallicity. Another solution consistent with the data is an older population ($\overline{t_M} \sim 2.6$ Gyr) with a longer star formation timescale ($\tau \sim 310$ Myr), larger dust attenuation ($A_v=0.6$ mag), and sub-solar metallicity.

And finally, another possible solution is characterized by an intermediate age population ($\overline{t_M} \sim 1.9$ Gyr) with very short star formation timescale ($\tau \sim 24$ Myr), larger dust attenuation ($A_v=0.7$ mag), and also sub-solar metallicity. We remark that all 3 solutions fit the data equally good, although we must warn the reader that most of the spectro-photometric data points are bluer than $1 \mu\text{m}$ rest-frame, so the fits are biased towards the bluer part of the SED.

In Figure 6, we show the procedure used to identify the three clusters of solutions in the t_0 - τ parameter space. We plot in the t_0 - τ space the solutions obtained for the 1000 Montecarlo simulations. The 3 clusters mentioned above can be identified by colors, and we also depict the median values of each solution.

We can understand how our results are affected by degeneracies by analyzing the properties of the clusters for the whole sample. We obtained 176 different solutions for the 104 galaxies in our sample. This means that each galaxy has, on average, 1.7 solutions. In fact, there are 48 galaxies ($\sim 46\%$ of the sample) for which we find only one cluster, i.e., only one set of properties fits the data, after taking into account observational uncertainties and the degeneracies linked to them. There are 41 galaxies (39%) with 2 clusters of solutions and less than 15% of the sample has 3 or more clusters (with the maximum number of clusters being 4, which happens for two galaxies).

We derived the maximal difference of the galaxy parameters obtained for the different solutions for each galaxy. The mean relative differences are $\delta t_0 \sim 40\%$, $\delta \overline{t_M} \sim 30\%$, $\delta \tau \sim 80\%$, $\delta A_v=0.1$ mag, $\delta M \sim 0.1$ dex. The differences between different solutions for the stellar masses and the dust attenuations are of the order of the typical uncertainties of each cluster of solutions, meaning that they are not strongly affected by the degeneracies. In fact, only two galaxies with degenerate solutions present δA_v values larger than 0.5 mag. The degeneracies in t_0 are smaller than 50% in relative values (even smaller, 30%, for the $\overline{t_M}$). The τ differences are larger for the degenerate solutions. Again, the metallicity uncertainties could not be determined because the allowed Z values are discrete. The metallicity values are unique (i.e., $\delta Z=0$) for 55% of the galaxies with more than one cluster of solutions.

3.3 Using spectral indices and IR detections to break degeneracies

The SED fitting technique described in the previous section does not make use of the full power of the dataset gathered for this work. Including all photometric data points from the UV to the mid-IR gives us the global shape of the stellar emission. But this global shape may easily wash out the higher spectral information given by the spectro-photometric data from SHARDS and the grism observations. Thus, the stellar population properties can be even better constrained when taking advantage of the ultra-deep spectro-photometric SHARDS and grism data. The high resolution ($R \sim 50$) photometry from SHARDS and the grisms allows us to measure spectral indices such as M_{gUV} and D4000, which are well correlated to stellar population properties such as the age (Kauffmann et al. 2003; Daddi et al. 2005).

We measure the M_{gUV} index presented in Daddi et al. (2005) as a strong age-dependent feature in the UV, detectable in relatively low resolution spectra in the region 260-290 nm. This feature is an absorption band formed by a combination of several strong Mg and Fe lines. The M_{gUV} index is defined as:

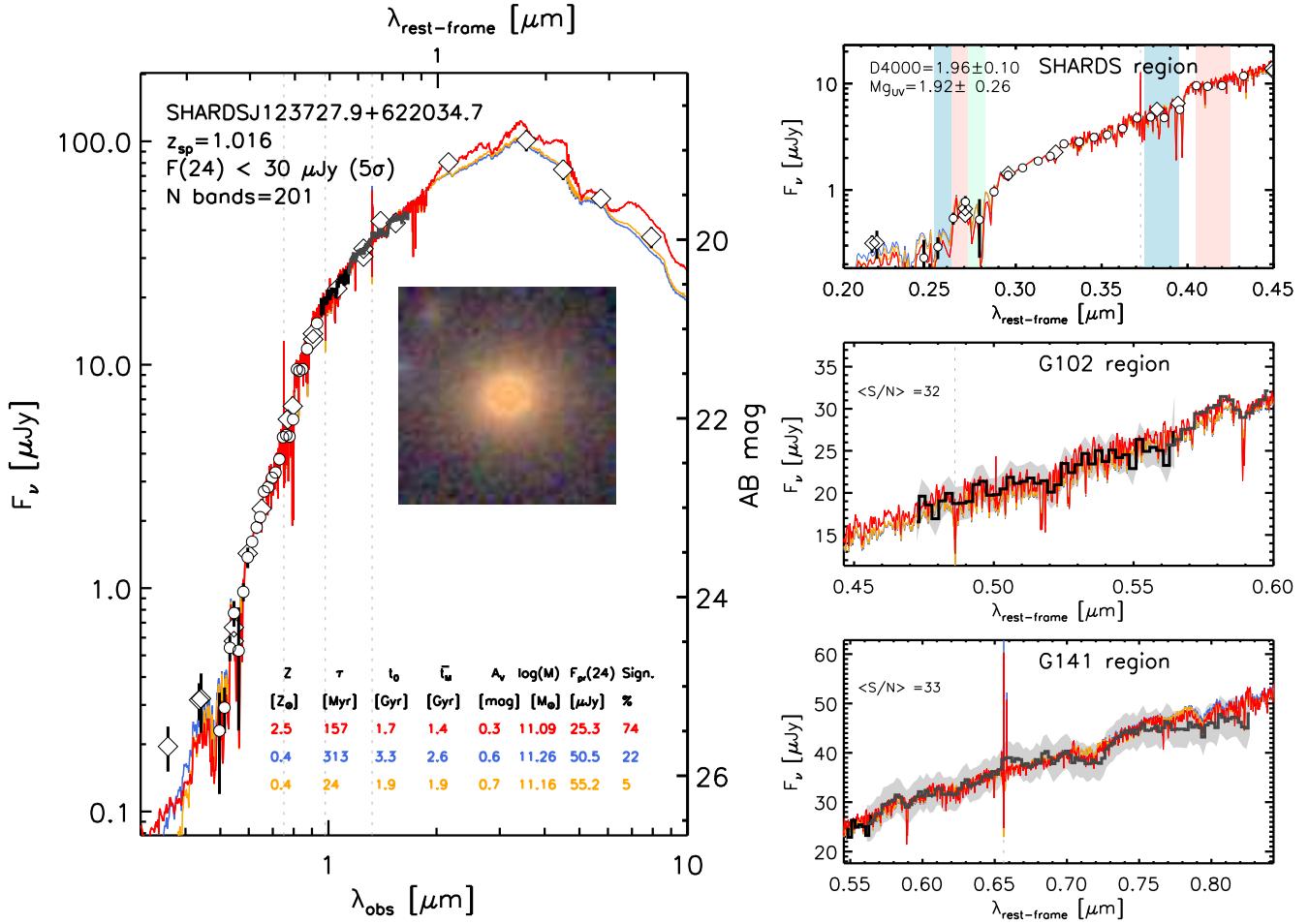


Figure 5. Example of our SED-fitting method, including the analysis of degeneracies, for SHARDSJ123620.3+6200844.3, a galaxy at $z_{sp} = 1.016$. Colors and symbols as in Figure 4. For this galaxy, three clusters of solutions were obtained after applying the method described in Section 3.2. The main parameters of each solution are shown in the legend.

$$Mg_{UV} = \frac{2 \times \int_{262.5}^{272.5} f_\lambda d\lambda}{\int_{252.5}^{262.5} f_\lambda d\lambda + \int_{272.5}^{282.5} f_\lambda d\lambda} \quad (7)$$

where the integration ranges are defined in nm. Note that to measure the Mg_{UV} index we need 10 nm windows, which at redshift $z > 1$ translates to 20 nm or more. This means that the SHARDS filters, with a typical width around 16 nm, present a sufficient spectral resolution to measure the Mg_{UV} absorption index.

We also measured the D4000 index, introduced by Bruzual (1983), which gives an estimate of the strength of the 4000 Å break. This index is defined as:

$$D4000 = \frac{\int_{405.0}^{425.0} f_\nu d\nu}{\int_{375.0}^{395.0} f_\nu d\nu} \quad (8)$$

where the integration ranges are again defined in nm.

We prefer to use this definition instead of the narrow index D_n4000 (Balogh et al. 1999) to reduce the uncertainty measurement of the index using photometric data alone, thanks to the broader index bands. See Hernán-Caballero et al. (2013) for more details about measuring D4000 and D_n4000 with SHARDS data.

To measure the spectral indices based on our spectrophotometric data, we first selected the data points for each galaxy that fall into each band of the index definition. These bands depend on the redshift of the galaxy, but we note that for SHARDS we have to consider the position of the galaxy in the FOV, given that the central wavelength of the pass-band seen by each galaxy depends on the position in the OSIRIS focal plane (see Pérez-González et al. 2013). We directly measured the ratios between the corresponding fluxes to get a first estimation of the indices. We refer to these index measurements as Mg_{UV}^* and $D4000^*$. To be able to compare these values with the typical index definitions, we correct them by using the ratio between the index measured in the best-fitting model of each galaxy at the central wavelength of each filter convolved to the SHARDS resolution and the standard index (defined in Eq. 7 and 8) measured directly in the models. The typical value of this correction is small, the average is 1.11 for Mg_{UV} , and 0.99 for D4000. We also checked that the correction is rather insensitive to the use of only one stellar population model to measure the correction, i.e., using a larger set of models with different timescales and ages has very small effect ($\leq 10\%$). We remark that the indices calculated in this way are completely independent of the SED-fitting procedure and are based on the observed photometric data alone.

In Figure 6, we plot a zoom of the SED around the spectral

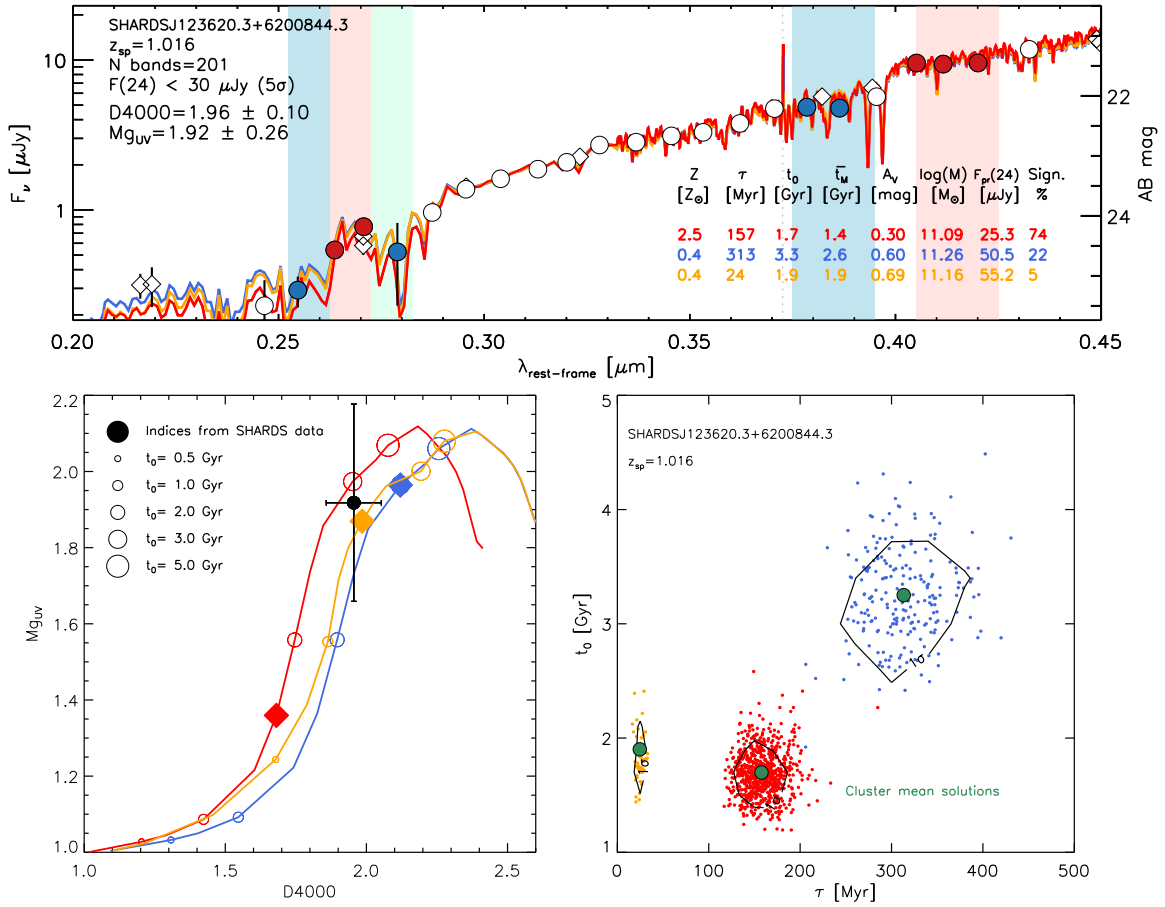


Figure 6. Example of the procedure used to break degeneracies among best-fitting solutions using measurements of absorption indices. *Upper panel:* we show a zoom of the SED, centered in the SHARDS region, for the same galaxy depicted in Figure 5. The shaded bands mark the regions used to measure the Mg_{UV} and D4000 indices. The colored circles represent the data points used to measure the indices from the SHARDS photometry. *Lower left panel:* we show the evolutionary tracks in the Mg_{UV} -D4000 plane for the 3 best-fitting models found for SHARDSJ123620.3+6200844.3. The empty circles show the expected values for the indices at different ages (from smaller to larger symbols: 0.5, 1.0, 2.0, 3.0 and 5.0 Gyr). The large colored diamonds show the location of the indices at the age of the best-fitting solution. The black circle represents the indices measured from the SHARDS photometry. *Lower right panel:* Distribution of the 1000 best-fitting solutions in the age/timescale plane for SHARDSJ123620.3+6200844.3. Note that this is the direct age from the SED-fitting (t_0) and not \bar{t}_M . The colored dots correspond to each one of the identified clusters, with the same color as in the SED plot. For each one of the 3 clusters, the median values are represented by large green circles and the black contours enclose 68% of the solutions.

range covered by SHARDS for the galaxy presented in Figure 5. The bands used to derive the spectral indices are marked as shaded regions. In the lower left panel, we plot the corrected Mg_{UV} and D4000 indices for that particular galaxy as well as the tracks expected for the evolution of these indices according to the models of the 3 best-fitting (degenerated) solutions obtained for that galaxy (see Section 3.2). The index measurements for this galaxy allowed us to eliminate solutions which are incompatible with the spectrophotometric data. For this particular galaxy, the measured indices are more compatible with the second and third solutions, and we discard the most significant solution (the one with $t_0 \sim 1.7$ Gyr).

In addition to the use of spectral indices, we evaluated the robustness of the different solutions obtained for each galaxy by making use of the (un-)detection in the mid- and far-IR and imposing an energy balance. For each best-fitting solution, given the dust attenuation and mass, we derived the expected flux at an observed wavelength of $24\mu\text{m}$ ($F_{pr}(24)$, for the galaxy shown in Figure 4, the values are written in the legend). The procedure starts calculating the luminosity absorbed by dust in the UV/optical, which has to be

re-emitted in the IR. We assumed that the stellar emission absorbed by dust must be equal to the IR luminosity integrated from 8 to $1000 \mu\text{m}$, L_{IR} . We then used the Rujopakarn et al. (2013) relation to transform the L_{IR} into a $24 \mu\text{m}$ observed flux (a relation that depends on redshift). For galaxies undetected in the IR, we were able to eliminate solutions which present expected $24 \mu\text{m}$ fluxes larger than the detection limit ($\sim 50 \mu\text{Jy}$ at 50% completeness). For example, for the SHARDSJ123620.3+6200844.3, the third solution predicts a $24 \mu\text{m}$ flux of $\sim 55 \mu\text{Jy}$. As this galaxy is not detected in the IR, we rejected the third solution and chose as the best solution the second one ($\bar{t}_M \sim 2.6$ Gyr, $\tau = 300$ Myr). With this method, we were able to reject only $\sim 4\%$ of the degenerate solutions, but it was a strong argument to limit the attenuation range probed by our stellar population analysis to values within $0 < A_V < 1.5$ mag. Larger values would imply IR detections for galaxies as massive as ours.

When all the solutions for a galaxy are compatible with the measured indices and do not violate the energy balance argument, we choose the most significant one, i.e., the most populated cluster. We were able to break the degeneracies making use of the spec-

tral indices for $\sim 32\%$ of the galaxies with more than one cluster of solutions. For the remaining objects, the indices uncertainties were too large (due to photometric errors) or the indices predicted by the tracks of all the different solutions were consistent with the measured values. We choose the most significant solution in $\sim 32\%$ of the cases. For 20% of the galaxies, the solutions were very similar in $t - A_v - Z$, with only significant differences in τ . We also discarded 7% of the solutions for being unrealistic ($\tau \leq 10$ Myr and $\log(M/M_\odot) \geq 11.0$).

In summary, out of the complete sample of 104 galaxies, 46% of them had only one possible solution (i.e., no degeneracies). For another $\sim 20\%$ we were able to break the degeneracies either by measuring absorption indices or by using the MIR/FIR data. For the remaining $\sim 34\%$, we used the most significant solution. In the next sections, we will only consider one solution for each galaxy and we will refer to them as primary solutions.

4 THE STAR FORMATION HISTORIES OF MQGS

In this Section, we analyze the properties of the stellar populations of MQGs at $1.0 < z < 1.5$. For the discussion, we only consider the primary solutions identified with the methodology described in Section 3.

4.1 Statistical properties of the stellar populations in MQGs

In Figure 7, we show the location of our galaxies in the mass-weighted age vs. mass ($\bar{t}_M - M$) plane, color-coded using 3 bins in star formation timescale. The τ bins have been chosen at the values where the \bar{t}_M/τ relation changes trend. We also show the relationship between \bar{t}_M and τ , color-coded using 3 bins of mass. The mass bins limits are approximately the median and 3rd quartile values. The population of MQGs at $z = 1.0 - 1.5$ are dominated by “new arrivals”, i.e., galaxies with relatively young stellar populations: $\bar{t}_M < 2$ Gyr. About 85% of the sample is that young. We also identify a tail of old galaxies ($\bar{t}_M > 2$ Gyr) accounting for $\sim 15\%$ of the total population. The derived properties of the MQGs are correlated among them, although with significant scatter. Hereafter, to better understand the MQGs, we divide them in three sub-samples depending on their \bar{t}_M values: *mature* ($\bar{t}_M < 1.0$ Gyr, 38 objects), *intermediate* ($\bar{t}_M = 1.0 - 2.0$ Gyr, 50 objects), and *senior* ($\bar{t}_M > 2.0$ Gyr, 16 objects) galaxies. The statistical properties of the galaxies divided in age and mass bins are listed in Table 2.

The population of mature galaxies presents an average mass-weighted age $\langle \bar{t}_M \rangle = 0.8_{0.7}^{0.9}$ Gyr and relatively short timescales $\langle \tau \rangle = 60_{20}^{100}$ Myr. The typical mass is $\log(\langle M \rangle / M_\odot) = 10.4_{10.3}^{10.7}$. On the other side, the senior population presents average values of $\langle \bar{t}_M \rangle = 2.6_{2.2}^{3.4}$ Gyr, longer star formation timescales, $\langle \tau \rangle = 400_{300}^{500}$ Myr, and larger masses $\log(\langle M \rangle / M_\odot) = 10.7_{10.6}^{11.0}$. The intermediate population has transitional parameters: $\langle \bar{t}_M \rangle = 1.4_{1.2}^{1.7}$ Gyr, $\langle \tau \rangle = 200_{30}^{300}$ Myr and $\log(\langle M \rangle / M_\odot) = 10.5_{10.3}^{10.8}$.

Note that the fact that the mature population has short τ values is due to our sample selection. As we are selecting quiescent galaxies (galaxies with low levels of sSFR), galaxies with longer τ (> 100 Myr) and young ages (< 1 Gyr) would have too high sSFR values to enter in our quiescent sample selection. In principle, the senior galaxies might present short or long star formation timescales, i.e., we do not have any selection bias against any of those types of galaxy. The bias of our results due to our sample selection are further discussed in Sect. 4.3, together with the mean SFH for the mature, intermediate, and senior galaxies.

With respect to the dust attenuation, the senior galaxies are less dusty, $\langle A_v \rangle = 0.4_{0.1}^{0.6}$, than the mature ones, $\langle A_v \rangle = 0.8_{0.5}^{1.1}$. The attenuation values are in agreement with those found by other authors (e.g., Belli et al. 2015). The galaxies with the highest dust attenuations are among the youngest ($\sim 90\%$ of the galaxies with $A_v > 0.8$ mag are younger than 2 Gyr), indicating that they could be post-starburst galaxies where the dust did not have time to disperse or disappear yet. With respect to the metallicities, 41% of the galaxies are best-fitted with solar metallicity, 36% with super-solar metallicity and 23% with sub-solar metallicity. No clear metallicity trends are found by analyzing the metallicity distributions in mass or ages bins.

At this point, we want to mention the difference between old and quiescence when using τ models. In SSP models, all the star formation takes place at the formation time of the galaxy, and then the population passively evolves. Therefore, an old galaxy is always quiescent and, in fact, a young galaxy would be also literally quiescent (although it may be not selected with our criteria). When using τ models, the duration of the star formation depends on τ . Galaxies with long star formation timescales may have been formed more than 1-2 Gyr ago but could be still forming stars. What actually indicates the sSFR of a galaxy (and consequently the star formation activity/quiescence) is the age/ τ relation.

In Figure 8, we show again the \bar{t}_M vs. τ plot, but now the galaxies are color-coded on the basis of their sSFR_{SED} (calculated from the best-fitting models, i.e., these sSFRs are different from those used in the selection, which were based in the observed UV luminosity and attenuation estimates –see Section 2.2–). The galaxies with similar sSFR_{SED} values are distributed along diagonal lines of constant \bar{t}_M/τ values. The senior population of galaxies with long τ values shows higher sSFR values than mature galaxies with very short τ . The size of the symbols represents the percentage of mass assembled in the last Gyr. Obviously, the mature galaxies ($\bar{t}_M < 1$ Gyr) assembled 100% of their mass during that time (by definition of mature objects). There is a population of intermediate galaxies with $\tau > 100$ Myr that has assembled between 10-50 % during the last Gyr, while the senior population has assembled less than 10 % of its mass. We also differentiate in Figure 8 between *UVJ*-selected and sSFR-selected galaxies. sSFR-selected objects, i.e., galaxies outside the quiescent *UVJ*-region (or inside the *UVJ*-quiescent region but detected in the IR), are preferentially located in the lower right corner of the \bar{t}_M - τ plane. This indicates that the sSFR-selected galaxies (which fall outside the *UVJ* region by definition) have larger \bar{t}_M/τ values and are less quiescent than the pure *UVJ* galaxies. In Table 3 we show the median properties of each sub-sample and we discuss the distribution of the derived galaxy properties in the *UVJ*-plot in Section 4.2 and Figure 11.

Our result about a duality (mature vs. senior systems) in the population of MQGs at $1.0 < z < 1.5$ and their differences not only in ages but also in timescales and attenuation was tested. The test was planned to check that the population of old (> 2 Gyr) massive quiescent galaxies at $z = 1.0 - 1.5$, which is just a 15% and a tail in the age distribution, is real, and its existence is not an effect of the degeneracies (in the τ - \bar{t}_M plane). For this purpose, we constructed spectro-photometric stacks for the mature ($\bar{t}_M < 1.0$ Gyr), intermediate ($\bar{t}_M = 1.0 - 2.0$ Gyr) and senior ($\bar{t}_M > 2.0$ Gyr) populations.

The broad-band colors of the three sub-samples of galaxies are very similar (they were selected with the same method based on colors) in the whole wavelength range. However, at the resolution achieved by the spectro-photometric data from SHARDS and the WFC3 grisms, especially in the Mg_{UV} and D4000 spectral regions, the sub-samples and the average fitting models show

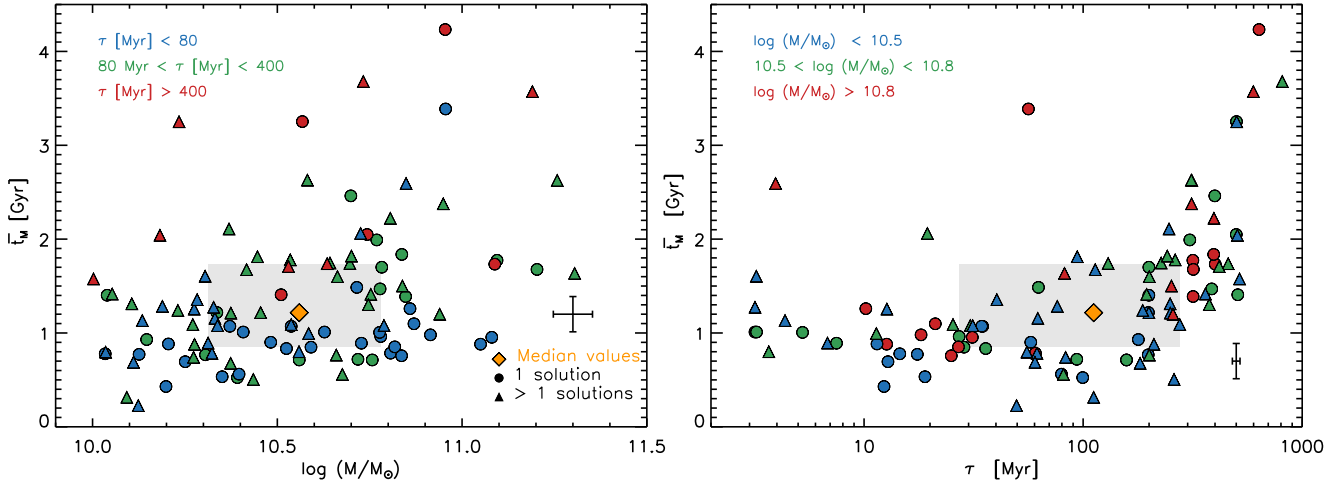


Figure 7. Mass-weighted ages versus stellar mass (*left panel*) and star formation timescale (*right panel*). Galaxies are color coded by star formation timescale and mass in each plot, respectively. Only the primary solutions (those selected with the different methods described in Sections 3.2 and 3.3) are plotted. Circles represent galaxies with only one solution, while triangles represent galaxies with degenerate solutions. The gray area represent the region between the 1st and 3rd quartiles for each parameter, and the yellow diamond is the median value. Typical uncertainties are plotted in the lower right corner of each plot.

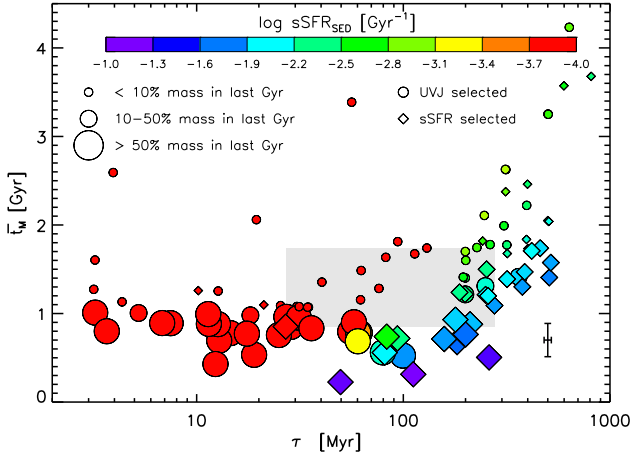


Figure 8. Mass-weighted ages versus star formation timescale. Galaxies are color coded by their sSFR_{SED} . Circles represent *UVJ*-selected galaxies, while the squares are *sSFR*-selected. The sizes of the symbols represent the percentage of mass assembled in the last Gyr. The gray areas represent the region between the 1st and 3rd quartiles. Typical uncertainties are plotted in the lower right corner.

measurable differences. In Figure 9, we show the stellar population models with the mean properties of the mature and senior populations, concentrating in the spectral region covered by SHARDS. There are significant differences in the relative fluxes for the two models, especially in the Mg_{UV} and D4000 regions. Therefore, we should be able to distinguish between the two solutions by measuring these indices, and this is possible in the SHARDS and grism data (and not with broad-band observations).

In the left panels of Figure 10, we present the stacks built for the mature and senior galaxy populations together with the models with their average properties. In the right panel of Figure 10, we show the indices measured in the stacks of the mature, intermediate and senior galaxy populations. We also show the model tracks for the stellar population models characterized by the average timescales and attenuations quoted in Table 2 for each sub-population. We demonstrate that the spectro-photometric data directly show the differences in the stellar population properties for the 3 sub-samples. Note that the origin of the average stellar popu-

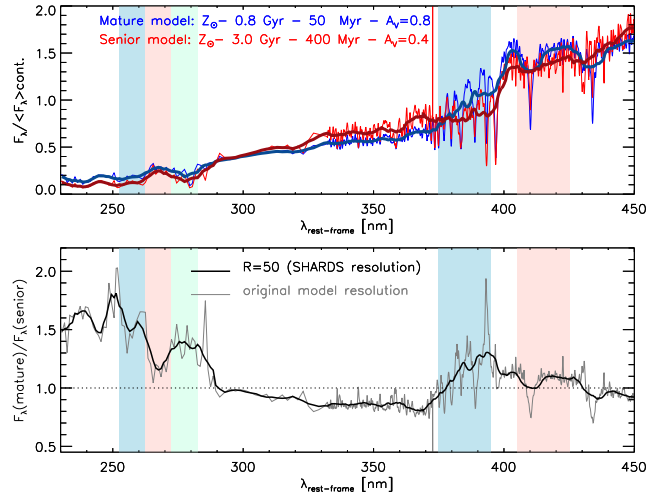


Figure 9. Differences of the average stellar population models for the mature and senior galaxy sub-samples (see text for details) at the resolution of our SHARDS+grism dataset ($R \sim 50$). *Upper panel*: stellar population models with the average properties of the mature and senior populations (as shown in the legend) in the spectral region covered by SHARDS. The models have been normalized to the fluxes in the 230–450 nm range. We show both the original resolution of the models (thin lines) and the models convolved to the SHARDS resolution ($R=50$, thick lines). *Lower panel*: ratio of the two models shown above at the original model resolution (thin gray line) and at $R=50$ (thick black line). We remark the significant (and measurable) differences between the two models at the resolution of our spectro-photometric data, especially for the Mg_{UV} and D4000 indices (marked in both plots as colored areas).

lation properties is the full-SED spectral fits, and here we are comparing those models with finer resolution data in a limited wavelength range. The two analysis are not completely independent, but the information encoded in the data at the resolution which makes index measurements possible could easily be erased or degraded by fitting the whole SED from the UV to the mid-IR. Our test demonstrates that we are seeing differences in the galaxy populations in both the global SED and the spectral indices. We, thus, conclude

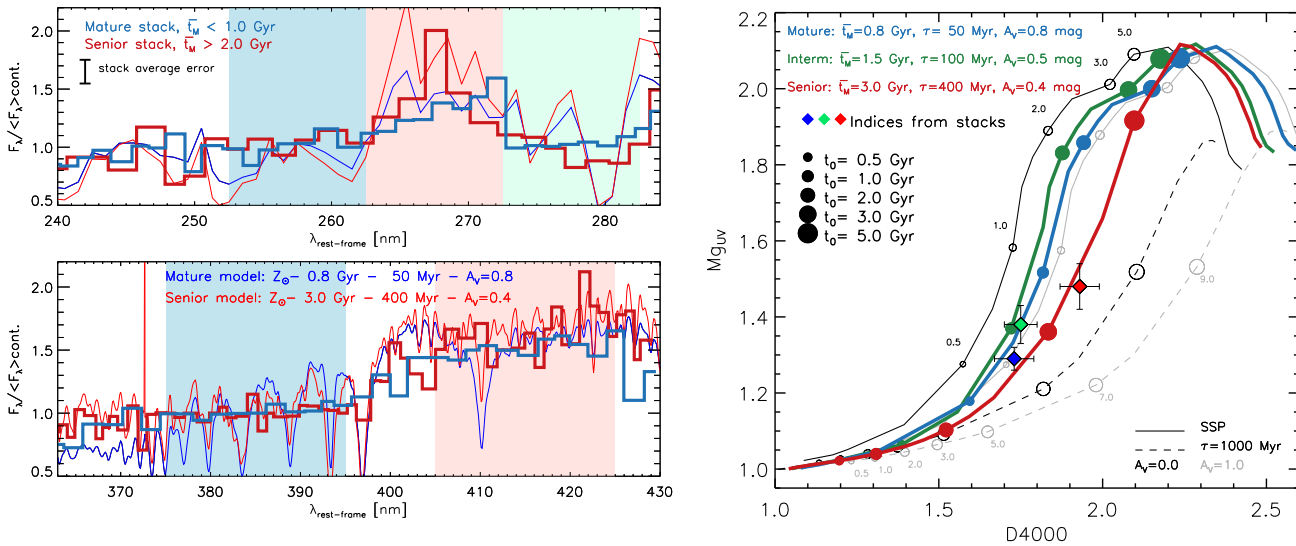


Figure 10. *Left panel:* Stacks for the senior (thick red line) and mature (thick blue line) populations normalized in the Mg_{UV} (upper panel) and D4000 regions (lower panel). The average error of the stacks is $\sim 10\%$. We also plot the normalized models with the mean properties of each stack (thin lines). *Right panel:* Mg_{UV} vs. D4000 plane with measurement in the stacks for the mature, intermediate, and senior galaxies (blue, green and red diamonds with error bars). For comparison, we also show the evolutionary tracks for 2 models with different star formation timescales (a single stellar population, SSP, and a delayed exponential model with $\tau=1000$ Myr) and two different dust attenuations ($A_V=0.0$ mag and $A_V=1.0$ mag). The empty circles represent the expected index values for each track at different ages (given in Gyr in the plot). The three colored lines show the tracks of the models corresponding to the mean properties of each galaxy population (given in the legend), with the filled colored circles marking index values for different ages (0.5, 1.0, 2.0, 3.0, 5.0 Gyr). The indices measured in the stacks are compatible with the average properties derived from the SED-fitting.

that our results about the ages of MQGs at $z = 1.0 - 1.5$ are robust and not an artifact linked to the stellar population degeneracies.

The longer timescale for the senior galaxies, which are also relatively massive, is not directly consistent with a typical conception in the *downsizing* scenario which states that the most massive galaxies formed their stars early but also very rapidly. A short timescale for the formation of massive galaxies has also been claimed to be necessary to explain the α -element enhancement seen in early-type massive galaxies (such as ellipticals) in the nearby Universe (see, e.g., Thomas et al. 2005 and Renzini 2006). Our estimations of the timescales for the most massive galaxies are not extremely large (typically 400 Myr) and would be rightly consistent with the values needed to match the chemical abundances (see Worthey et al. 1992; Worthey 1998 and references therein). In addition, these massive galaxies may be the product of mergers (or clumps) involving progenitors with shorter timescales, but with different ages, maybe linked to small offsets (of the order of tens or a few hundred Myr) in the ignition of the star formation. The SFHs obtained for the merged systems (i.e., our galaxies) would then present larger timescales, but do not violate any constrain linked to α -element enhancement. In Section 4.3, we further discuss the mean SFH of our galaxies as a function of the mass and age and the importance of selection effects.

The variety in the ages of quenched galaxies at $z = 1.0 - 1.5$ is in agreement with previous works such as Bedregal et al. (2013) and Belli et al. (2015). Both papers present a wide range of stellar population properties for similar samples as ours. Bedregal et al. (2013), analyzing the G102-G141 WFC3 grisms of 41 massive ($\log(M/M_\odot) > 10.65$ M_\odot) quiescent galaxies at $z \sim 1.5$ found that they have exponentially declining SFH with short star formation timescales ($\tau \leq 100$) and a wide distribution in stellar ages (1–4 Gyr). Belli et al. (2015) analyzed Keck LIRS spectra of quiescent

galaxies at $1.0 < z < 1.6$ with $\log(M/M_\odot) > 10.6$ M_\odot and concluded that there are two different quenching routes. The youngest galaxies ($t \sim 1$ Gyr) show a fast quenching ($\tau \sim 100$ Myr), while the older galaxies (up to 4 Gyr old) show slowly-declining SFHs ($\tau \geq 200$ Myr). Note, however, that our τ values and theirs are not directly comparable, since we used different parametrizations for the SFH (i.e., the τ parameter for an exponential is not exactly the same as the τ value for a delayed exponential).

4.2 Dissecting the UVJ diagram: distribution of stellar population properties

In Figure 11, we plot the UVJ color diagram, which was the starting point of our selection, to study how the UVJ colors do actually correlate with the derived galaxy properties. The main properties of the UVJ - and sSFR-selected sub-samples are shown in Table 3. We recall that we refer to UVJ -selected to galaxies in the quiescent region of the UVJ diagram and without IR detection, while the sSFR-selected have $sSFR < 0.2$ Gyr^{-1} but are located outside the passive UVJ region or they are detected in the IR (see Sect. 2.2).

Concerning ages, there is not a significant difference between those derived for the UVJ -selected and sSFR-selected samples. The average ages are $\langle t_M \rangle = 1.1_{0.9}^{1.7}$ and $1.2_{0.8}^{1.7}$ Gyr for each sub-sample, respectively. However, the senior galaxies seem to have redder $V - J$ colors (with average values $V - J = 1.46_{1.32}^{1.50}$) than the mature population ($V - J = 1.31_{1.15}^{1.39}$).

The timescales are more clearly segregated in the UVJ plot. The τ of the UVJ -selected galaxies are shorter than those of the sSFR-selected galaxies: typical $\langle \tau \rangle$ values are 60_{20}^{200} Myr and 250_{160}^{400} Myr, respectively. Comparing our results with those in Belli et al. (2015), who also presented stellar population proper-

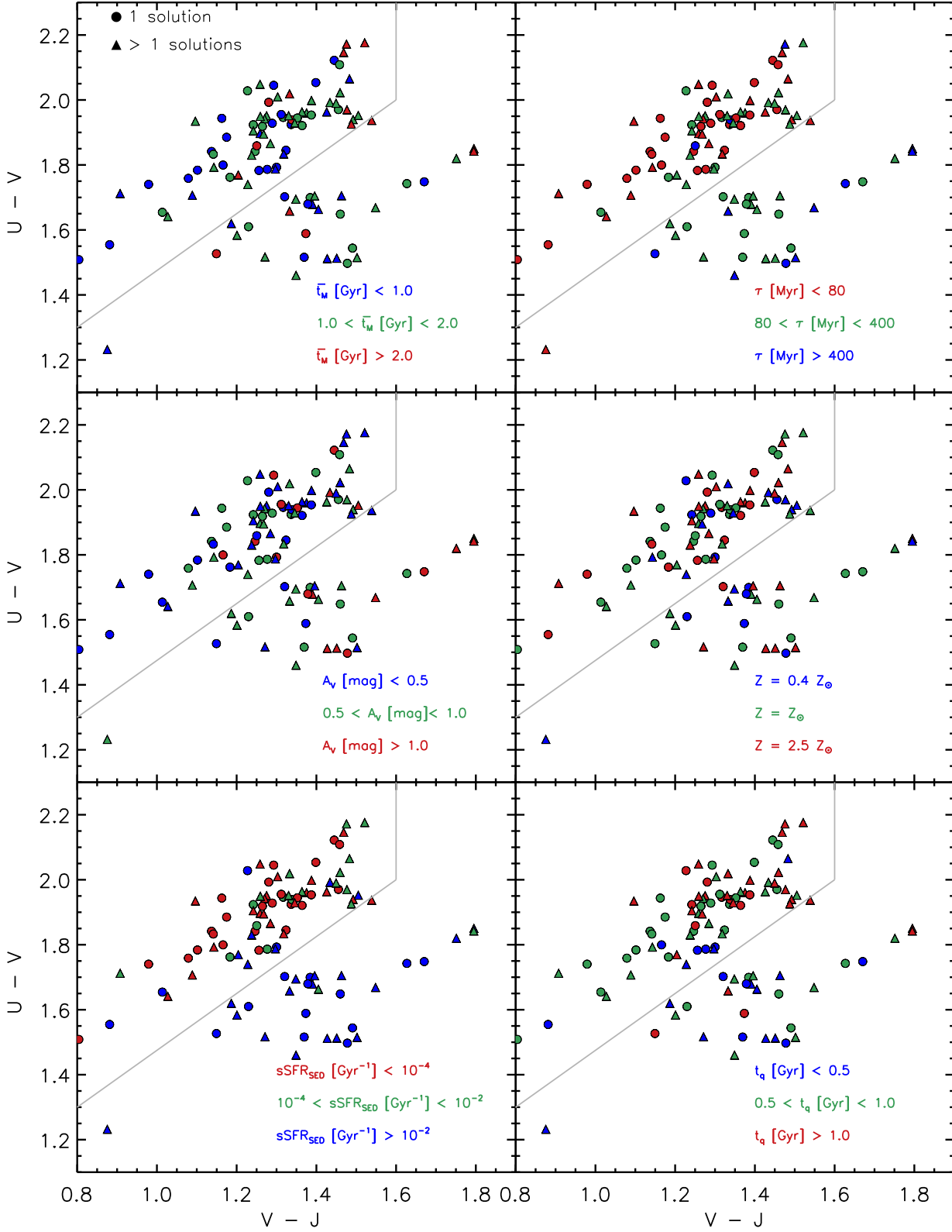


Figure 11. UVJ diagrams with galaxies color coded on the basis of different properties: mass-weighted age \bar{t}_w , star formation timescale τ , attenuation A_v , metallicity Z , SED-based specific star formation rate $sSFR_{SED}$, and quenching time t_q . The circles represent galaxies with no degenerate solutions, while the triangles are galaxies with more than one solution in the Monte Carlo simulations (see Section 3.2). UVJ -selected galaxies are located inside the quiescent region of each diagram, while $sSFR$ -selected galaxies fall outside by definition (see sect. 2.2, Table 3).

Parameter	sub-sample	Q1	Median	Q3
t_0 [Gyr]	Mature (N=38)	0.8	0.9	1.0
	Interm. (N=50)	1.3	1.8	2.2
	Senior (N=16)	3.0	3.2	4.2
	Low Mass (N=45)	0.9	1.1	1.6
	Interm. Mass (N=36)	1.0	2.0	2.3
	High Mass (N=23)	1.0	2.0	3.0
τ [Myr]	Mature	20	60	100
	Interm.	30	200	300
	Senior	300	400	500
	Low Mass	20	80	200
	Interm. Mass	30	200	400
	High Mass	30	250	300
A_v [mag]	Mature	0.5	0.8	1.1
	Interm.	0.1	0.5	0.8
	Senior	0.1	0.4	0.6
	Low Mass	0.2	0.6	1.0
	Interm. Mass	0.3	0.6	0.9
	High Mass	0.3	0.5	0.8
Z/Z_\odot	Mature	1.0	1.0	2.5
	Interm.	0.4	1.0	2.5
	Senior	0.4	1.0	1.0
	Low Mass	1.0	1.0	2.5
	Interm. Mass	1.0	1.0	2.5
	High Mass	1.0	1.0	1.0
$\log(M/M_\odot)$	Mature	10.3	10.4	10.7
	Interm.	10.3	10.5	10.8
	Senior	10.6	10.7	11.0
	Low Mass	10.1	10.3	10.4
	Interm. Mass	10.6	10.7	10.8
	High Mass	10.8	10.9	11.0
$\overline{t_M}$ [Gyr]	Mature	0.7	0.8	0.9
	Interm.	1.2	1.4	1.7
	Senior	2.2	2.6	3.4
	Low Mass	0.8	1.1	1.3
	Interm. Mass	1.0	1.4	1.8
	High Mass	1.0	1.6	2.4
$sSFR_{SED}$ [Gyr $^{-1}$]	Mature	$<10^{-4}$	$<10^{-4}$	10^{-2}
	Interm.	$<10^{-4}$	10^{-3}	10^{-2}
	Senior	10^{-3}	10^{-3}	10^{-2}
	Low Mass	$<10^{-4}$	10^{-4}	10^{-2}
	Interm. Mass	$<10^{-4}$	10^{-3}	10^{-2}
	High Mass	$<10^{-4}$	10^{-3}	10^{-2}
t_q [Gyr]	Mature	0.2	0.5	0.7
	Interm.	0.7	0.9	1.1
	Senior	1.5	1.9	2.6
	Low Mass	0.4	0.6	0.9
	Interm. Mass	0.7	0.9	1.2
	High Mass	0.8	1.0	1.7

Table 2. Galaxy properties of our sample separated in mature ($\overline{t_M} < 1.0$ Gyr) intermediate ($1.0 < \overline{t_M} < 2.0$ Gyr) and senior ($\overline{t_M} > 2.0$ Gyr) and mass bins: $\log(M/M_\odot)=[10.0,10.5]$, $\log(M/M_\odot)=[10.5,10.8]$ and $\log(M/M_\odot)=[10.8,11.4]$. We show the 1st, median and 3rd quartiles for the best-fitting ages (t_0), star formation timescales (τ), dust attenuations (A_v), metallicity (Z), masses (M), mass-weighted ages ($\overline{t_M}$), $sSFR_{SED}$ and quenching time (t_q , explained in Sect. 4.2)

Parameter	sub-sample	Q1	Median	Q3
t_0 [Gyr]	<i>UVJ</i> (N=65)	0.9	1.1	2.0
	<i>sSFR</i> (N=39)	1.0	1.7	2.5
τ [Myr]	<i>UVJ</i>	20	60	200
	<i>sSFR</i>	160	250	400
A_v [mag]	<i>UVJ</i>	0.1	0.5	0.8
	<i>sSFR</i>	0.4	0.7	1.1
Z/Z_\odot	<i>UVJ</i>	1.0	1.0	2.5
	<i>sSFR</i>	0.4	1.0	2.5
$\log(M/M_\odot)$	<i>UVJ</i>	10.3	10.5	10.8
	<i>sSFR</i>	10.3	10.7	10.8
$\overline{t_M}$ [Gyr]	<i>UVJ</i>	0.9	1.1	1.7
	<i>sSFR</i>	0.8	1.2	1.7
$sSFR_{SED}$ [Gyr $^{-1}$]	<i>UVJ</i>	$<10^{-4}$	$<10^{-4}$	10^{-3}
	<i>sSFR</i>	10^{-2}	10^{-2}	10^{-1}
t_q [Gyr]	<i>UVJ</i>	0.7	0.9	1.2
	<i>sSFR</i>	0.3	0.6	1.0

Table 3. Galaxy properties of our sample separated by their selection criteria (*UVJ*/*sSFR*, see Sect. 2.2). The parameters are the same as those in Table 2.

ties within the *UVJ* diagrams, we find a similar trend: they see that galaxies with $\tau < 100$ Myr were distributed in a narrow region parallel to the diagonal line defined in the *UVJ* passive region.

Belli et al. (2015) also found that galaxies with higher dust attenuations ($A_v \sim 1$ mag) were outside the passive region. We find typical $\langle A_v \rangle = 0.5_{0.1}^{0.8}$ and $\langle A_v \rangle = 0.7_{0.4}^{1.1}$ mag for the *UVJ*-selected and *sSFR*-selected galaxies, respectively, in good agreement with Belli et al. (2015). The percentage of *UVJ*-selected galaxies with $A_v > 1$ mag is only 7%, while this percentage increases up to 28% for the *sSFR*-selected galaxies. With respect to the metallicity, no clear trends are present for neither of the two selection criteria. The fraction of *UVJ*-selected galaxies with sub-, solar and super-solar metallicity is 20, 40 and 40 %, respectively. For the *sSFR*-selected the percentages are 25, 46 and 30 %. We note that, if the metallicity was a fixed parameter (e.g., solar metallicity), the galaxy properties would be better segregated within the *UVJ* diagram, as the *UVJ* colors would be constrained by only 3 parameters instead of 4. In Figure 11, we also present how SED-based *sSFRs* correlate with the position in the *UVJ* diagram. The most quiescent galaxies are located in a similar region to the galaxies with low τ values. In fact, $\sim 60\%$ of the *UVJ*-selected galaxies have $\log(sSFR_{SED}) < -5$ Gyr $^{-1}$, while this only happens for $\sim 8\%$ of the *sSFR*-selected galaxies.

We have also derived the quenching time, defined as the time since the galaxy became quiescent using our definition from Section 2.2, i.e., how much time has passed since the galaxy had $sSFR_{SED} < 0.2$ Gyr $^{-1}$. The *UVJ*-selected galaxies have been dead, on average, for almost 1 Gyr ($\langle t_q \rangle = 0.9_{0.7}^{1.2}$ Gyr), while the *sSFR*-selected galaxies have been more recently quenched ($\langle t_q \rangle = 0.6_{0.3}^{1.0}$ Gyr).

4.3 Characterization of the SFHs of MQGs

In this Section we analyze the SFHs for MQGs at $1.0 < z < 1.5$ in the observed redshift range and at higher lookback times. One of the advantages of determining SFHs with stellar population models is that they provide us with a time-dependent evolution of param-

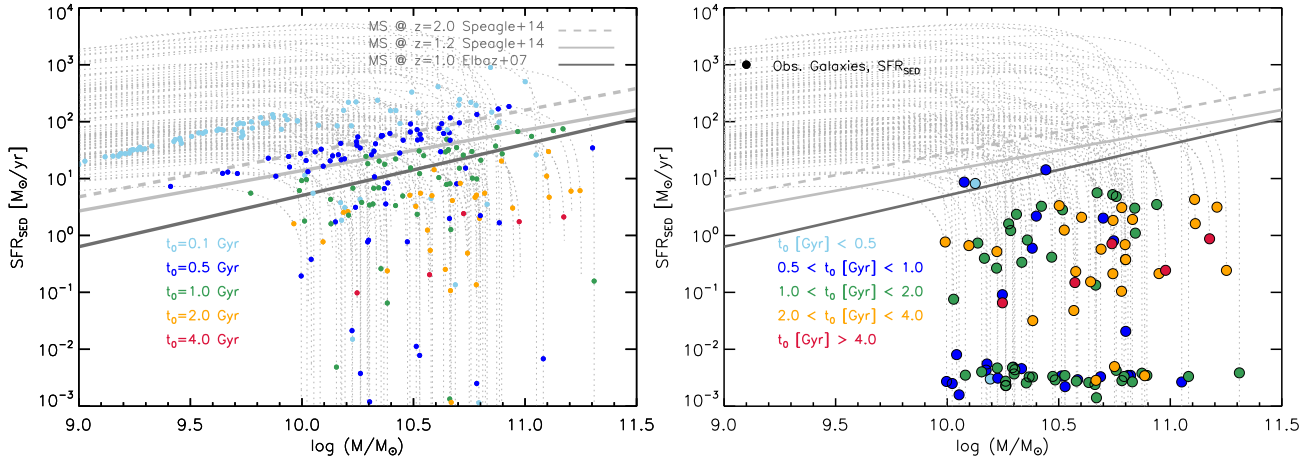


Figure 12. Evolutionary tracks in the SFR_{SED} -Mass plane for our sample of MQGs. *Left panel:* the small dots mark the location of each galaxy at different times after their formation, as indicated in the legend. Note that these are direct ages from the models and we have assumed the same origin for all SFHs. We mark as dotted lines the past path for each galaxy. The gray lines show the location of the main sequence at $z \sim 1.2$ and $z \sim 2$ according to Speagle et al. (2014), and at $z \sim 1$ according to Elbaz et al. (2007). Most of the galaxies are ~ 0.5 - 1.0 Gyr old when they are on the MS region at $z > 1.0$, i.e., our MQGs take about 1 Gyr to leave the MS and become quiescent. *Right panel:* Location of our galaxies in the SFR_{SED} -Mass plane at the epoch of observation (large filled circles), color-coded by their best-fitting ages. We note that both the ages and SFRs used in this plot are the output of the SED-fitting (and not SFR_{UV} neither \bar{t}_M). To better visualize the location of the galaxies in the SFR_{SED} -Mass plane, we plot galaxies with very low $\text{SFR}_{\text{SED}} \sim 10^{-3} M_{\odot} \text{yr}^{-1}$.

ters such as the SFR and the galaxy stellar mass. Therefore, assuming closed-box evolution (i.e., no merging events or re-activation of the star formation activity), we do not only characterize the properties of a given galaxy at the epoch of observation, but we can also trace back its properties and see how it assembled its mass at earlier cosmic times.

One of the most fundamental relations between galaxy properties is the SFR-Mass relation, the so-called main sequence (MS). In Figure 12 we show the evolutionary paths of the galaxies in our sample in the SFR_{SED} -Mass plane as a function of time. For this plot, we assumed that all galaxies started their formation at the same time (i.e., all SFHs share the $t=0$ point). The shape of the track depends mainly on the final mass and the star formation timescale τ : galaxies with short timescales form the bulk of their mass very quickly, they arrive relatively early to the MS and then their star formation decreases while their stellar mass remains almost unchanged (falling almost vertically). Galaxies with very large τ values continuously increase their mass without changing their SFR (horizontal tracks) and may stay in the MS for ~ 2 Gyr. According to our derived SFHs (note that the choice of the parametrization is also important), after 100-500 Myr of evolution our galaxies would form a MS with very similar slope to that observed directly at $z > 1$ with samples of star-forming galaxies (see, e.g., Speagle et al. 2014). We remark that, for this exercise, we offsetted the SFHs of our sample to make them match at $t=0$. The effect of galaxies starting their formation at different epochs would result in a widening of the main sequences shown in Figure 12 for different ages. According to our results, galaxies would come out of the MS after approximately 1 Gyr, and quenching would then proceed almost vertically in this plot. Therefore, we find that MQGs would pass a fair fraction of their lifetimes in the MS, with the possibility to live above the MS (in the starburst locus) for short periods of time of the order of 100 Myr. We conclude that the SFHs we have determined for MQGs at $1.0 < z < 1.5$ are consistent with the slope and even the location of the MS at $z > 1$, and that the concept of the MS is mainly an age effect.

At this point, we also want to remark that the current SFR_{SED} for many of our galaxies (averaged over the last 100 Myr of their

history) derived from the SED modeling is much smaller than the SFR obtained from observables. The current SFR_{SED} are not fully consistent for the UV luminosities corrected for attenuation, or L_{IR} measurements, as we explained in Section 2.1 and used in the sample selection. Indeed, 45 % of the sample have $\text{SFR}_{\text{SED}} < 10^{-3} M_{\odot} \text{yr}^{-1}$ but the lowest SFR estimated from the typical tracers is $10^{-0.5} M_{\odot} \text{yr}^{-1}$. This could be due to an overestimation of the dust attenuation from the IRX- β relation, but the choice of a delayed exponentially decreasing SFH is most probably responsible for most of this effect. Typically, this parametrization produces very low SFRs for dead galaxies (whose emission is dominated by an evolved stellar population), but there might exist a second stellar population with some (very low and negligible in terms of mass and emission) on-going star formation which would not be possible to recover with the assumed SFH parametrization. However, the fits of the model to our data are very good for all the sample and the inclusion of a second population would multiply by 2 the uncertainties and degeneracies. We, therefore, assume that our galaxies are dominated by the older stellar population and one (composite) stellar population model explains the main features of our galaxies. We caution the reader, however, that the current SFR_{SED} should be taken as lower limits.

Following Kennicutt (1998), we can derive the SFR corresponding to LIRGs/ULIRGs: $L_{\text{IR}}=10^{11} L_{\odot}$ corresponds to $12 M_{\odot} \text{yr}^{-1}$, and $L_{\text{IR}}=10^{12} L_{\odot}$ to $121 M_{\odot} \text{yr}^{-1}$ (transformed to Kroupa IMF). All of the galaxies in our sample had SFR peaks larger than the LIRG limit (except for one galaxy which has $\log(M/M_{\odot})=10.0$). The typical fraction of their lifetime spent in the LIRG phase is $\sim 32\%$ (~ 500 Myr). A significant fraction of the sample (46%) had SFR peaks larger than the ULIRG limit, but the typical fraction of their lifetime in this phase is much smaller, $\sim 8\%$ (~ 100 Myr). Our results favor LIRGs at $z > 1.5$ as the most likely progenitors of MQGs at $1.0 < z < 1.5$, and that most of their stars were formed in star-forming events with SFRs around $100 M_{\odot} \text{yr}^{-1}$. The ULIRGs seem to be the progenitors of the most massive galaxies. The fraction of galaxies which have undergone a ULIRG phase increases up to 65% and 75% when considering

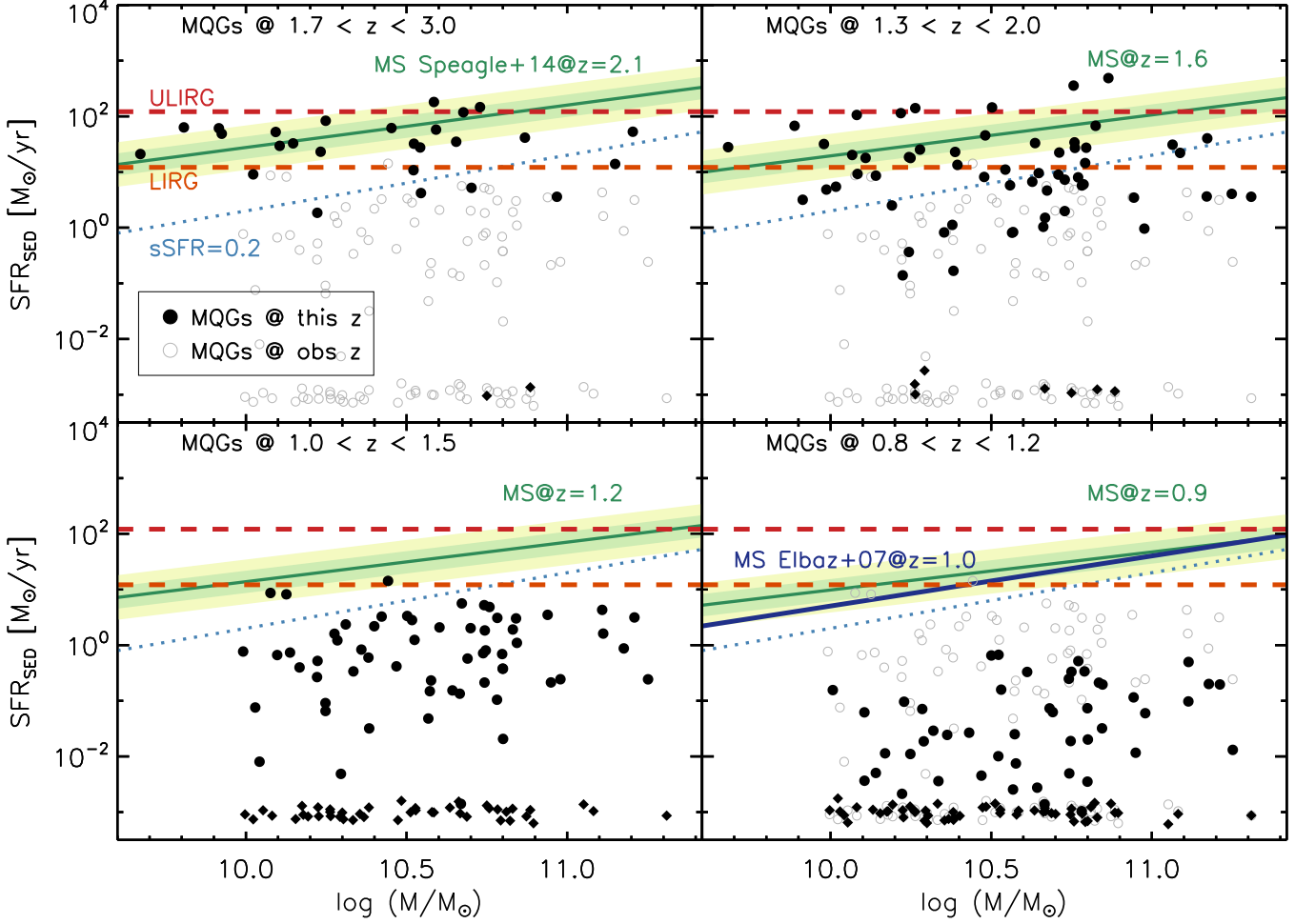


Figure 13. Evolution of the MQGs in the SFR_{SED} -Mass plane at different redshifts. The observed properties (those measured directly in the data) are plotted as black filled circles in the redshift bin $z = 1.0 - 1.5$ (“the present”) and as gray empty circles in the other panels. The expected location of the galaxies 1 Gyr ($z = 1.3 - 2.0$) and 2 Gyr ($z = 1.7 - 3.0$) before the observations are plotted as black filled circles in the upper right and upper left panels, respectively. The lower right panel represents the expected location of the galaxies 1 Gyr after the observations ($z = 0.8 - 1.2$). We use the age, timescale, mass and SFR given by our SED fits to move forward and backwards in time in the SFR_{SED} -Mass diagram, assuming passive evolution. For comparison, we plot as a green line the MS from Speagle et al. (2014). The dark and light green areas mark the 1σ and 2σ scatter, 0.2 and 0.4 dex. The blue line in the $z = 0.8 - 1.2$ panel is the MS from Elbaz et al. (2007). The red/orange lines show the SFR limit for LIRGs/ULIRGs converted into SFRs using Kennicutt (1998) relation. The light blue dotted line is the value of constant sSFR used in the selection (see Sect. 2.2; $sSFR = 0.2 \text{ Gyr}^{-1}$). Galaxies with $SFR_{SED} < 10^{-3} M_{\odot} \text{ yr}^{-1}$ are plotted as black diamonds at $SFR_{SED} \sim 10^{-3} M_{\odot} \text{ yr}^{-1}$.

galaxies with masses larger than $10^{10.8} M_{\odot}$ and $10^{11.0} M_{\odot}$, respectively.

In Figure 13, we show where our galaxies would be placed in the SFR_{SED} -Mass plane at different redshifts in their past and future history. We study 4 redshift bins corresponding to 2 and 1 Gyr before the observations, the actual observed redshift and 1 Gyr after the observations. In Table 4, we show the percentages of galaxies above, within, and below the MS at different redshifts. Figure 13 shows that at $1.0 < z < 1.5$, the epoch of observation, all of our galaxies lie 1σ below the MS (this happens also when using the SFRs based on classical tracers), as expected given that we started with a selection of passive galaxies. If we move 1 Gyr backwards in time, $\sim 23\%$ of the galaxies are located in or above the MS, but a significant number fraction ($\sim 78\%$) of the galaxies at $z \sim 1.6$ are located below the MS, meaning that they were already quiescent.

z bin	MS+ 2σ	MS+ 1σ	MS	MS- 1σ	MS- 2σ
1.7 – 3.0	N=8 12%	N=10 15%	N=5 7%	N=52 78%	N=46 69%
1.3 – 2.0	N=2 7%	N=7 23%	N=8 27%	N=15 50%	N=12 40%
1.0 – 1.5	–	–	–	N=104 100%	N=101 97%
0.8 – 1.2	–	–	–	N=104 100%	N=104 100%

Table 4. Number and percentage of galaxies above (1 or 2σ), in and below (1 or 2σ) the MS from Speagle et al. (2014) at each redshift bin, as show in Figure 13.

At $z \sim 2.1$, the bulk of the galaxies cannot be plotted because $\sim 70\%$ have best-fitting ages smaller than 2 Gyr, so at that epoch they were not formed yet (or, most probably, their masses were much smaller than our limits in the plot). At that redshift bin, half of the galaxies (50%) are in the MS or above but the other half (15 galaxies) are 1σ below the MS. In the opposite time direction, if we move 1 Gyr after the observations, all of our galaxies have very low SFR_{SED} and are completely dead and well below the MS from Speagle et al. (2014) and Elbaz et al. (2007).

Comparing with the parent population of galaxies more massive than $10^{10} M_{\odot}$ at each redshift bin, we find fractions of quiescent galaxies of 25, 12 and 3% at $z = 1.0 - 1.5$, $z = 1.3 - 2.0$ and $z = 1.7 - 3.0$, respectively. Different studies have shown that the fraction of quiescent galaxies constantly increases with time. For example, Domínguez Sánchez et al. (2011) derived a fraction of quiescent galaxies ($\log(M/M_{\odot}) > 10.6$, $\text{sSFR} < 0.01 \text{ Gyr}^{-1}$) of ~ 20 and 10% at $z = 1.4 - 1.6$ and $z = 1.6 - 2.0$ respectively. The percentage found in Ilbert et al. (2013) for a sample of quiescent galaxies selected by their *NUV-r vs r-J* colors with $\log(M/M_{\odot}) > 9.6$ increases from 6% to 13% from $z = 2.5 - 3.0$ to $z = 1.1 - 1.5$. The evolution of the fraction of quiescent galaxies (*UVJ* selected) in Muzzin et al. (2013) is not so strong (28% at $z = 1.0 - 1.5$ and 24% at $z = 2.0 - 2.5$), although the mass limits used in this calculation change for each redshift bin, $\log(M/M_{\odot}) > 9.48$ at $z = 1.0 - 1.5$, $\log(M/M_{\odot}) > 10.54$ at $z = 2.0 - 2.5$. The fractions of MQGs that we derive at $z > 1.5$ by studying the past evolution of MQGs at $z = 1.0 - 1.5$ are consistent with observational results at higher densities.

In the next paragraphs, we compare the number density of quiescent galaxies in our work with a compilation of estimations from the literature. The number density of quiescent galaxies in our work for $z > 1.5$ are derived considering our results for the SFHs of $1.0 < z < 1.5$ MQGs and the position of the galaxies in a SFR_{SED} -Mass plot at different epochs. In this case, we assume that galaxies evolve passively once their star formation is quenched and they do not experience any merger event. We warn the reader that a fair comparison of number densities requires taking into account the differences in quiescent fraction linked to the stellar mass cut or the definition of quiescence, which vary from paper to paper and are very difficult to consider in their full extent. Here we consider a galaxy as quiescent when is located 1σ below the MS at each redshift. With this method, the number densities of MQGs from our work are $\rho = (7.0 \pm 0.7) \times 10^{-4} \text{ Mpc}^{-3}$ at $z = 1.0 - 1.5$, $\rho = (2.3 \pm 0.3) \times 10^{-4} \text{ Mpc}^{-3}$ at $z = 1.3 - 2.0$, and $\rho = (0.31 \pm 0.08) \times 10^{-4} \text{ Mpc}^{-3}$ at $z = 1.7 - 3.0$. This is in good agreement with the number densities of quiescent galaxies reported in Muzzin et al. (2013) at $z = 1.0 - 1.5$ ($\rho = 7.6 \times 10^{-4} \text{ Mpc}^{-3}$), but smaller than their number densities at higher redshifts $\rho = (3.3, 1.2, 0.65) \times 10^{-4} \text{ Mpc}^{-3}$ at $z = 1.5 - 2.0$, $z = 2.0 - 2.5$ and $z = 2.5 - 3.0$, respectively. There are several factors that could be affecting this comparison. In the first place, the redshift bins are not exactly the same. Besides, Muzzin et al. (2013) selection is only based on *UVJ* colors, while we are considering as quiescent galaxies 1σ below the MS at each redshift, as derived from the backwards evolution of the MQGs at $z = 1.0 - 1.5$. We recall that we have eliminated from our MQGs at $z = 1.0 - 1.5$ galaxies detected in the IR in the quiescent *UVJ* region, when they have $\text{sSFR} > 0.2 \text{ Gyr}^{-1}$. We also note that galaxies in the quiescent region of the *UVJ* diagram at $z = 1.7 - 3.0$ can have much larger sSFR (up to 1.0 Gyr^{-1}) than our quiescent limit. We recall that the values derived for the past evolution of MQGs must be taken with care, as we are assuming pure passive evolution and no merger events (which could help to decrease the number density of quiescent sources).

We also derive the number densities of our observed galax-

ies ($z = 1.0 - 1.5$) for the different populations defined in Sect. 4.1 (mature, intermediate, senior). This is shown in Figure 14, together with the number density of Muzzin et al. (2013) at $z = 1.0 - 1.5$ and Whitaker et al. (2013). The existence of a population of old ($t > 1.3 \text{ Gyr}$) galaxies at $z \sim 2$ has already been found by Whitaker et al. (2013) after analyzing the stellar populations of 171 massive *UVJ*-selected galaxies using stacked 3D-HST spectra. Given that in this work they use SSP models and we use more general (and realistic) delayed exponential models, the comparison with our sample is not straight forward, but we compare their results with our mass-weighted ages. Taking into account that the age of the universe at $z \sim 1.7$ is 1.2 Gyr younger than at the epoch we consider in this study ($z \geq 1.2$), the galaxies observed by Whitaker et al. (2013) would be $\sim 2.5 \text{ Gyr}$ old at the redshifts probed in our work, should they stay passive and not re-ignite. In our sample, we find a number density of galaxies with $\bar{t}_M > 2.0$ of $1.1 \pm 0.2 \times 10^{-4} \text{ Mpc}^{-3}$ for $\log(M/M_{\odot}) > 10.50$ and $0.9 \pm 0.2 \times 10^{-4} \text{ Mpc}^{-3}$ for $\log(M/M_{\odot}) > 10.5$. This results are consistent within errors with the number density of *UVJ* galaxies from Whitaker et al. (2013) ($0.8 \pm 0.1 \times 10^{-4} \text{ Mpc}^{-3}$) at $z = 1.4 - 2.2$ and with $\log(M/M_{\odot}) > 10.50$. The similar number densities from Whitaker et al. (2013) for MQGs with ages around 1.5 Gyr at $z \sim 2$ and those obtained in this work with ages $\sim 2.5 \text{ Gyr}$ at $z \sim 1.3$ is a good consistency check on the existence of old galaxies at $z > 1.5$. However, this value is smaller than the number density of Muzzin et al. (2013) at $z = 1.5 - 2.0$ for galaxies with $\log(M/M_{\odot}) > 10.50$ ($\rho \sim 1.9 \times 10^{-4} \text{ Mpc}^{-3}$). This difference could be due to the more restrictive selection from Whitaker et al. (2013), where the authors require G141 WFC3/HST grism detection for their sample. Given the discrepancies on previous results and the difficulty in making a fair comparison between number densities, it is difficult to reach firm conclusions regarding the assembly of the red sequence. However, the number densities (and fractions of quiescent galaxies) that we find when considering passive galaxies at $z = 1.0 - 1.5$ and moving back in time seem to be consistent or smaller than those reported in studies based on galaxies at those actual redshifts above $z = 1.5$. This could suggest that mergers play an important role or that the SFH of galaxies could be more complicated than the delayed exponentially declining assumed in this work (i.e., with the re-ignition of the star-formation for some galaxies).

In Figure 15 we show the evolution of the ages of MQGs over the last 10 Gyr. We compare our results with previous works based on stacked spectra (Mendel et al. 2015; Whitaker et al. 2013; Onodera et al. 2014; Schiavon et al. 2006; Choi et al. 2014) and individual spectral measurements (Belli et al. 2015; Barro et al. 2015). We compare the data with the predictions from pure passive evolution of a delayed τ -models with different formation redshifts. The median ages derived for our sample ($\bar{t}_M \sim 1.2 \text{ Gyr}$) are consistent with those from Belli et al. (2015) at the same redshift. The ages derived for the senior population could be explained in terms of passive evolution of the galaxies studied in Mendel et al. (2015); Whitaker et al. (2013); Onodera et al. (2014) and Barro et al. (2015) at higher redshifts, suggesting that at least part of the quiescent population at higher redshift do not restart their star formation once they are quenched. However, the number density of old ($> 2 \text{ Gyr}$) MQGs is very small and the average properties of MQGs are dominated by galaxies with ages $< 2 \text{ Gyr}$.

The observed properties of $z < 1$ galaxies are not fully consistent with a pure passive evolution of our sample of MQGs at $z \sim 1.2$. If the mature population evolved passively, they would have typical ages consistent with those derived for the most massive galaxies ($\log(M/M_{\odot}) \sim 11.3$) of the Choi et al. (2014) sample at $z < 1$. How-

ever, the median mass of the mature population is ~ 10.4 , meaning that they should grow by almost 0.9 dex in mass in 3-5 Gyr to be consistent with Choi et al. (2014) results. Recent works suggest that galaxies can increase their mass by a factor of ~ 2 due to residual SFR (e.g. Pérez-González et al. 2008; Fumagalli et al. 2014) or via major mergers (Shankar et al. 2015), which is not enough to account for this mass discrepancy. The masses of the senior population ($\log(\langle M \rangle / M_\odot) = 10.7$) would be consistent with the most massive sample of Choi et al. (2014), suggesting that they could be the progenitors of $z < 1$ MQGs. In this case, some level of rejuvenation should take place since $z \sim 1.2$, in order to reconcile the ages of our sample with those from Choi et al. (2014). SFH with larger star formation episodes ($\tau > 400$ Myr) could also help alleviating the discrepancies. On the other hand, the properties of the less massive ($\log(M/M_\odot) \sim 10.7$) quiescent galaxies at $z < 1$ from Choi et al. (2014) cannot be explained in terms of passive evolution of quiescent galaxies at higher- z , suggesting that the less massive population is still forming stars at $z > 1$.

The relatively uniform ages (around 1-2 Gyr) measured at $z > 1$ suggest that the quiescent galaxy population is being kept young by the constant addition of recently quenched galaxies, i.e., “new arrivals”, as we mentioned in Section 4.1 and was already stated in previous studies (e.g. Mendel et al. 2015). We conclude that the formation of the red sequence of quiescent galaxies is actually occurring at $z = 1.0-2.0$ (no results are available beyond that redshift). At these redshifts, the number density of the oldest population is small and the population of dead galaxies is dominated by new arrivals with ages around 1-2 Gyr (or mature galaxies, as we defined them in this work). Only at redshifts below $z \sim 1$ the MQGs population is totally assembled and evolves passively with no significant new additions. This is in agreement with previous studies supporting a significant evolution of the number density of MQGs at lower redshifts: by a factor of ~ 2 from $z \sim 1.5$ down to $z \sim 0.7$, epoch at which the bulk of this population seems to be definitively assembled (see Daddi et al. 2005; Eliche-Moral et al. 2010; Davidzon et al. 2013; Prieto et al. 2013; Mendel et al. 2015; Prieto & Eliche-Moral 2015).

To study the dependence of the SFH with mass and age, we divide our sample in 3 mass bins in $\log(M/M_\odot)$ units: 10.0–10.5, 10.5–10.8, and 10.8–11.5; and also in 3 bins in \bar{t}_M : < 1 Gyr, 1–2 Gyr, > 2 Gyr (corresponding to the mature, intermediate and senior populations introduced in Section 4). We then construct the typical SFH for each sub-sample using the median τ and SFR_{max} values. The SFHs are normalized so that, by integrating them, we recover the median mass of each subsample. We also derive the mean age of the Universe when the galaxies were formed (t_{U-form}). We plot the results of the SFR_{SED} evolution for the three galaxy sub-samples divided by age and mass in Figure 16, and we give the obtained values in Table 5.

If we study the SFH of our sample divided in age bins (left panel of Figure 16), we find that the senior galaxies must have been formed, on average, when the Universe was only 2 Gyr old, while the intermediate and mature galaxies are formed when the Universe was 3.4 and 4.1 Gyr old, respectively. The age of the Universe when the galaxies had their maximum SFR is $t_{U \sim 2.3, 3.6, 4.2}$ Gyr with median $\text{SFR}_{max} = 60, 110, 230 M_\odot \text{ yr}^{-1}$ and median $\tau = 400, 200, 60$ Myr for the senior, intermediate and mature galaxies, respectively. This is a direct implication of the galaxy properties derived for each population and summarized in Table 2. According to this scenario, the senior MQGs would have been formed in a relatively young Universe in longer and not very intense star formation episodes, while, on the other hand, the recently quenched MQGs at $z = 1.0-1.5$

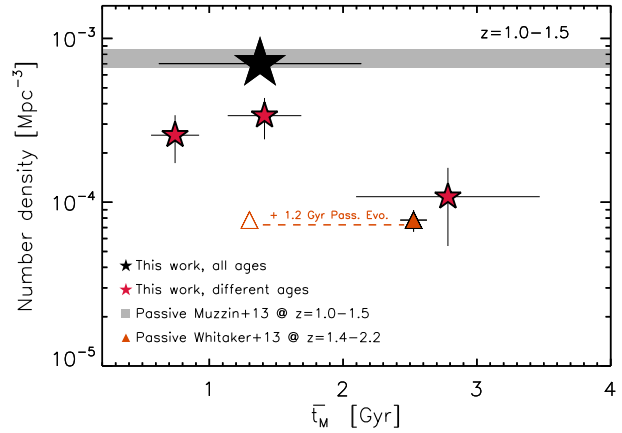


Figure 14. Number density of MQGs galaxies at $z = 1.0-1.5$ as a function of their mass-weighted age \bar{t}_M (red stars). The large black star is the total number density of MQGs from our work. We also show the number density of quiescent galaxies at the same redshift from Muzzin et al. (2013) (gray area). The orange empty triangle depicts the number density and mean age of MQGs at $z = 1.4-2.2$, as measured by Whitaker et al. (2013). Assuming passive evolution for these galaxies, these galaxies would move to the orange filled triangle. The number density uncertainties (shown as 2σ) have been calculated assuming Poisson statistics, while the error bars in age represent the standard deviation in each age bin.

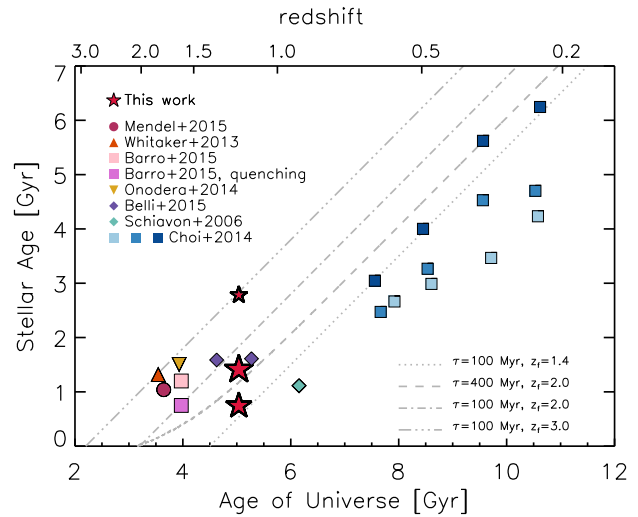


Figure 15. Evolution of the mean stellar age of MQGs over the last ~ 10 Gyr. The results from this work (red stars) are separated in 3 \bar{t}_M bins, the size of the symbols being proportional to the number density. The largest symbol is at $\bar{t}_M = 1.2$ Gyr, the mean age of our sample. Our results are compared with other SSP ages from the literature at different redshifts measured from stacks (Mendel et al. 2015; Whitaker et al. 2013; Onodera et al. 2014; Schiavon et al. 2006) or from individual spectra (Belli et al. 2015). We also plot the mean luminosity-weighted age for 3 quiescent galaxies and the luminosity-weighted age for a galaxy in the process of quenching derived in Barro et al. (2015). The results from Choi et al. (2014) at lower redshifts are divided in 3 mass bins, $\log(M/M_\odot) \sim 10.7, 11.0, 11.3$ from lighter to darker blue. The gray lines show the evolution of models with SFHs of the form $\text{SFR}(t) \propto t/\tau^2 \times e^{-t/\tau}$, with $\tau = 100$ Myr and different formation epochs ($z_f = 3.0, 2.0, 1.4$) and $\tau = 400$ Myr and $z_f = 2.0$.

Mass bins [$\log(M/M_\odot)$]	t_{U-form} (Gyr)	τ (Myr)	SFR_{max} (M_\odot/yr)
10.0 - 10.5	3.6	80	90
10.5 - 10.8	3.4	200	120
10.8 - 11.5	3.1	250	210

$\overline{t_M}$ bins [Gyr]			
< 1.0	4.1	60	230
1.0 - 2.0	3.4	200	110
> 2.0	1.9	400	60

Table 5. Median SFH of MQGs at $1.0 < z < 1.5$ divided in 3 mass bins and 3 $\overline{t_M}$ bins. We show the age of the Universe when the galaxies were formed (t_{U-form}), the star formation timescale (τ) and the maximal SFR (SFR_{max}) for each subsample.

must have been formed at later times in shorter and more intense bursts of star formation. We must notice that there are important selection effects in these results. The mature population must have been formed relatively quickly to be able to quench their star formation in less than 1 Gyr, meaning that they must present short τ values to satisfy our quiescent selection criteria.

With respect to the SFH divided in mass bins, the t_{U-form} was 3.6, 3.4 and 3.1 Gyr for the less massive, intermediate and most massive galaxies, respectively. There is a ~ 0.5 Gyr delay in the mean formation epoch of the least massive galaxies with respect to the most massive ones. This difference in time is larger than our age uncertainties (~ 0.2 Gyr), supporting that the most massive galaxies were formed first in time (in agreement with the downsizing scenario, Cowie et al. 1996). We derive that the peak of the SFR occurred at $t_U \sim 3.7, 3.6, 3.4$ Gyr with median $SFR_{max} = 90, 120, 210 M_\odot \text{ yr}^{-1}$ and median $\tau = 80, 200, 250$ Myr for the low, intermediate and high mass sub-samples, respectively.

We compare these results with the scenario proposed in Thomas et al. (2005, 2010) for the formation of massive galaxies based on data in the nearby Universe ($z \leq 0.06$), which established that the most massive galaxies ($\log(M/M_\odot) \sim 12$) formed 2 Gyr after the Big Bang in relatively short formation timescales ($\tau \sim 200$ Myr), while lower mass galaxies assembled later and had longer star formation episodes ($\tau > 1000$ Myr). The formation epoch of the galaxies in our sample takes place ~ 2 Gyr before Thomas et al. (2010) results in a similar mass range. However, a direct comparison with Thomas et al. (2010) work is not straight forward. We recall that we are limiting our study to $z = 1.0-1.5$, which restricts the latest formation epoch to $t_U - form \sim 6.0$ Gyr, while Thomas et al. (2010) sample considers local galaxies which could have been formed at $z < 1$. We do neither see the same mass-dependence with τ , but rather the opposite. Our τ uncertainties are quite large ($\sim 30\%$) and that the mass range analyzed in this work is limited to 1.5 orders of magnitude, which may be reducing the mass-dependence of the star formation timescales. But, more importantly, the median SFHs that we plot in Figure 16 are strongly affected by our selection criteria as we are only considering quiescent galaxies at $1.0 < z < 1.5$. This biases our sample against less massive galaxies with long star formation episodes (long τ) which were formed at $z \sim 1.2$ but are still forming stars. These galaxies did not have time to become quiescent at the redshift studied and therefore are not included in the average τ calculation of the less massive sample.

5 SUMMARY AND CONCLUSIONS

In this work, we have analyzed the Star Formation Histories (SFH) of 104 massive ($\log(M/M_\odot) > 10.0$) quiescent galaxies (MQGs) at $z = 1.0-1.5$. They were selected on the basis of their location in the quiescent region of the UVJ diagram (and no IR detection) or imposing a cut in the specific Star Formation Rate $sSFR < 0.2 \text{ Gyr}^{-1}$. We constructed the best possible Spectral Energy Distributions (SEDs) by combining SHARDS (Pérez-González et al. 2013) spectro-photometric data, HST/WFC3 G102 and G141 grisms, and multi wavelength ancillary data from the Rainbow database (Pérez-González et al. 2008; Barro et al. 2011). The SEDs were compared to delayed exponentially declining stellar population models and a Monte Carlo algorithm was used to characterize in detail the uncertainties and the inherent degeneracies in this kind of study.

Our main conclusions are:

- The combined use of SHARDS and WFC3/HST grism data represents a significant improvement in the study of MQGs at $z = 1.0-1.5$. These data allowed to characterize and even break degeneracies in some cases. For $\sim 50\%$ of our sample, we obtained a single solution in our analysis of the stellar population properties.
- Two spectral features, the Mg_{UV} and D4000 absorption indices, were found to be very useful to disentangle between the SED-fitting degeneracies in the other half of the sample. The spectral resolution of the SHARDS and grism data allowed us to break these degeneracies in $\sim 30\%$ of the cases where more than one model is consistent with the data.
- The MQGs at $z = 1.0-1.5$ present a wide range of properties, which are correlated between them. We divide our sample in 3 sub-populations based on their mass-weighted ages. Mature galaxies present ages $\overline{t_M} < 1$ Gyr, intermediate objects have $\overline{t_M} = 1-2$ Gyr, and senior galaxies are the oldest systems, $\overline{t_M} > 2$ Gyr. We find that mature galaxies have, on average, relatively short timescales, $\langle \tau \rangle = 60_{20}^{100}$ Myr, smaller masses, $\log(\langle M \rangle / M_\odot) = 10.4_{10.3}^{10.7}$, and large dust attenuations, $\langle A_v \rangle = 0.8_{0.5}^{1.1}$ mag. The senior population has longer star formation timescales, $\langle \tau \rangle = 400_{300}^{500}$ Myr, larger masses, $\log(\langle M \rangle / M_\odot) = 10.7_{10.6}^{11.0}$ and lower dust attenuations, $\langle A_v \rangle = 0.4_{0.1}^{0.6}$ mag. The intermediate population has transitional properties: $\langle \overline{t_M} \rangle = 1.4_{1.2}^{1.7}$ Gyr, $\langle \tau \rangle = 200_{50}^{300}$ Myr, $\langle A_v \rangle = 0.5_{0.1}^{0.8}$ mag and $\log(\langle M \rangle / M_\odot) = 10.5_{10.3}^{10.8}$.
- The global population of MQGs at $z = 1.0-1.5$ is dominated by new arrivals, 85% of the sample is younger than 2 Gyr (in mass-weighted age).
- The existence of such different populations has been tested by the measurement of spectral indices (Mg_{UV} and D4000) on the stacked data of each population. The indices values are consistent with those predicted by the tracks of the stellar population models with the average properties of each population, thus confirming that the derived properties are real and not a consequence of the degeneracies present in the SED-fitting.
- The UVJ color-color diagram segregates very well best-fitting properties such as τ or $sSFR_{SED}$. The UVJ -selected galaxies have short star formation timescales ($\tau \sim 60$ Myr) and low $sSFR_{SED}$ ($< 0.1 \text{ Gyr}^{-1}$). By complementing the MQGs with galaxies located outside the UVJ passive region but with $sSFR_{UV} < 0.2 \text{ Gyr}^{-1}$, we recover massive galaxies ($\log(M/M_\odot) \sim 10.68$) with old populations ($\overline{t_M} \sim 1.2$ Gyr) and longer star formation timescales ($\tau \sim 250$ Myr).
- Analyzing the derived SFHs, we studied the evolution of the SFR and mass as a function of time. We find that the tracks predicted by

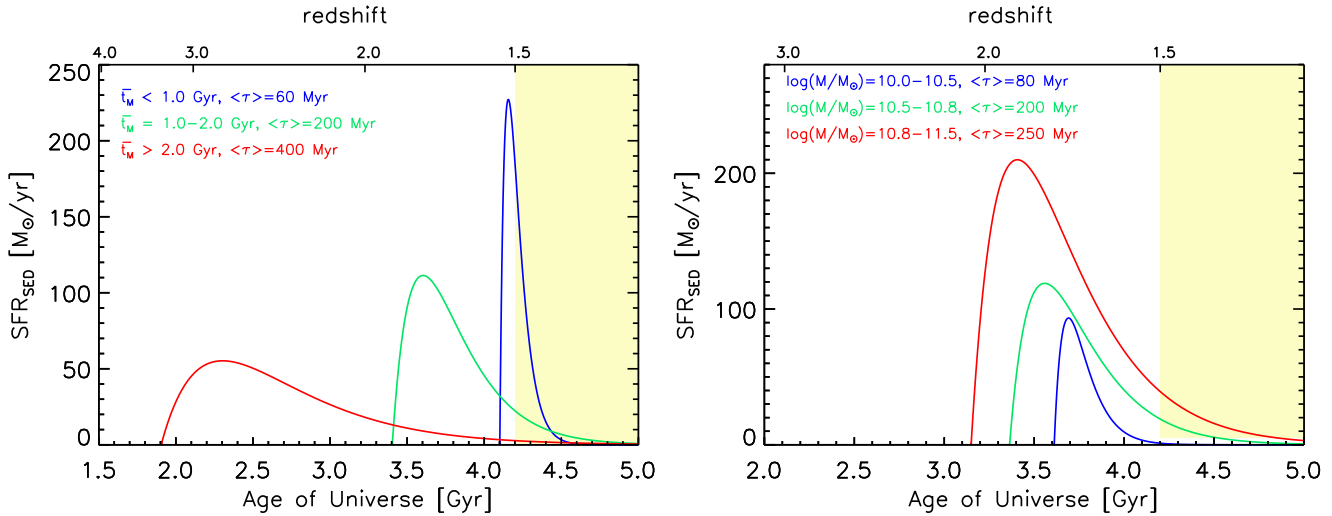


Figure 16. Average SFHs (SFR versus time) for our sample of MQGs divided in 3 age bins (*left panel*) and 3 mass bins (*right panel*). The yellow shaded area indicates the redshift studied in this work.

our SFHs are consistent with the slope and even the location of the main sequence of star-forming galaxies at $z > 1.5$.

- According to the SFHs that we derive, all the MQGs of our sample were LIRGs in the past, and 46% of them were ULIRG. The typical time spent in the LIRG/ULIRG phase was $\sim 500/100$ Myr ($\sim 32/8\%$ of their lifetime). The fraction of galaxies which have undergone a ULIRG phase increases up to 75% when considering galaxies with masses larger than $10^{11.0} M_{\odot}$, implying that the high- z ULIRGs may be the progenitors of the most massive passive galaxies.

- The number densities and ages derived for the senior MQGs are consistent with the passive evolution of quiescent galaxies at higher redshifts ($z \sim 2$), meaning that at least part of the quiescent population at $z \sim 2$ does not restart the star formation activity once they are quenched. However, at these redshifts, the number density of the oldest population is small and the population of dead galaxies is dominated by new arrivals with ages around 1-2 Gyr, i.e., the formation of the red sequence of quiescent galaxies is actually occurring at $z=1.0-2.0$. Only at redshifts below $z \sim 1$ the MQGs population is totally assembled and evolves passively with no significant new additions

- The median SFHs of our galaxies divided in 3 mass bins ($\log(M/M_{\odot})=10.0-10.5, 10.5-10.8, 10.8-11.5$) suggest that the most massive galaxies at $z=1.0-1.5$ were formed when the Universe was ~ 3 Gyr in intense ($SFR_{max} \sim 200 M_{\odot}yr^{-1}$) and relatively long ($\tau \sim 250$ Myr) star formation episodes, while the less massive galaxies are formed with a 0.5 Gyr delay in shorter ($\tau \sim 80$ Myr) and less intense ($SFR_{max} \sim 90 M_{\odot}yr^{-1}$) star formation processes.

- The median SFHs of our galaxies divided in 3 age bins suggest that the senior MQGs at $z=1.0-1.5$ would have been formed in a relatively young Universe ($t_U \sim 2$ Gyr) in long ($\tau \sim 400$ Myr) and not very intense star formation episodes ($SFR_{max} \sim 60 M_{\odot}yr^{-1}$), while, the mature MQGs must have been formed at later times ($t_U \sim 4$ Gyr) in shorter ($\tau \sim 60$ Myr) and more intense ($SFR_{max} \sim 230 M_{\odot}yr^{-1}$) bursts of star formation.

ACKNOWLEDGMENTS

We acknowledge support from the Spanish Programa Nacional de Astronomía y Astrofísica under grants AYA2012-31277. HDS

thanks Giovanni Zamorani for useful discussion. NCL acknowledges financial support from AYA2013-46724-P. AAH and AHC acknowledge support from the Spanish Programa Nacional de Astronomía y Astrofísica under grant AYA2012-31447, which is partly funded by the FEDER program. The work of AC is supported by the STARFORM Sinergia Project funded by the Swiss National Science Foundation. SC acknowledges support from the ERC via an Advanced Grant under grant agreement no. 321323-NEOGAL. This work has made use of the Rainbow Cosmological Surveys Database, which is operated by the Universidad Complutense de Madrid (UCM) partnered with the University of California Observatories at Santa Cruz (UCO/Lick,UCSC). Based on observations made with the Gran Telescopio Canarias (GTC) installed at the Spanish Observatorio del Roque de los Muchachos of the Instituto de Astrofísica de Canarias, in the island of La Palma. We thank all the GTC Staff for their support and enthusiasm with the SHARDS project.

REFERENCES

- Balogh M. L., Morris S. L., Yee H. K. C., Carlberg R. G., Ellingson E., 1999, *ApJ*, 527, 54
 Barro G. et al., 2015, *ArXiv e-prints*
 Barro G., Faber S. M., Pérez-González P. G. e. a., 2014, *ApJ*, 791, 52
 Barro G. et al., 2011, *ApJS*, 193, 13
 Bedregal A. G. et al., 2013, *ApJ*, 778, 126
 Bell E. F. et al., 2005, *ApJ*, 625, 23
 Belli S., Newman A. B., Ellis R. S., 2015, *ApJ*, 799, 206
 Bruzual A. G., 1983, *ApJ*, 273, 105
 Bruzual G., Charlot S., 2003, *MNRAS*, 344, 1000
 Buitrago F., Trujillo I., Conselice C. J., Bouwens R. J., Dickinson M., Yan H., 2008, *ApJ*, 687, L61
 Bundy K., Treu T., Ellis R. S., 2007, *ApJ*, 665, L5
 Calzetti D., Armus L., Bohlin R. C., Kinney A. L., Koornneef J., Storchi-Bergmann T., 2000, *ApJ*, 533, 682
 Choi J., Conroy C., Moustakas J., Graves G. J., Holden B. P., Brodwin M., Brown M. J. I., van Dokkum P. G., 2014, *ApJ*, 792, 95
 Cimatti A. et al., 2008, *A&A*, 482, 21

- Cimatti A., Daddi E., Renzini A., 2006, *A&A*, 453, L29
- Cimatti A. et al., 2004, *Nature*, 430, 184
- Cowie L. L., Songaila A., Hu E. M., Cohen J. G., 1996, *AJ*, 112, 839
- Daddi E. et al., 2005, *ApJ*, 626, 680
- Davidzon I. et al., 2013, *A&A*, 558, A23
- Domínguez Sánchez H., Pozzi F., Gruppioni C. e. a., 2011, *MNRAS*, 417, 900
- Elbaz D. et al., 2007, *A&A*, 468, 33
- Elbaz D., Dickinson M., Hwang H. S., Díaz-Santos T., Magdis G. e. a., 2011, *A&A*, 533, A119
- Eliche-Moral M. C. et al., 2010, *A&A*, 519, A55
- Elsner F., Feulner G., Hopp U., 2008, *A&A*, 477, 503
- Ferreras I. et al., 2012, *AJ*, 144, 47
- Ferreras I. et al., 2014, *MNRAS*, 444, 906
- Fontana A. et al., 2009, *A&A*, 501, 15
- Fumagalli M. et al., 2014, *ApJ*, 796, 35
- Gorgas J., Cardiel N., Pedraz S., González J. J., 1999, *A&AS*, 139, 29
- Grazian A. et al., 2015, *A&A*, 575, A96
- Grogin N. A. et al., 2011, *ApJS*, 197, 35
- Hernán-Caballero A. et al., 2013, *MNRAS*, 434, 2136
- Ilbert O., McCracken H. J., Le Fèvre O. e. a., 2013, *A&A*, 556, A55
- Ilbert O. et al., 2010, *ApJ*, 709, 644
- Kauffmann G. et al., 2003, *MNRAS*, 341, 33
- Kennicutt, Jr. R. C., 1998, *ApJ*, 498, 541
- Koekemoer A. M. et al., 2011, *ApJS*, 197, 36
- Kong X., Charlot S., Brinchmann J., Fall S. M., 2004, *MNRAS*, 349, 769
- Kriek M., van Dokkum P. G., Whitaker K. E., Labbé I., Franx M., Brammer G. B., 2011, *ApJ*, 743, 168
- Kroupa P., 2001, *MNRAS*, 322, 231
- Lilly S. J. et al., 2007, *ApJS*, 172, 70
- Madau P., Ferguson H. C., Dickinson M. E., Giavalisco M., Steidel C. C., Fruchter A., 1996, *MNRAS*, 283, 1388
- Marchesini D., van Dokkum P. G., Förster Schreiber N. M., Franx M., Labbé I., Wuyts S., 2009, *ApJ*, 701, 1765
- McCracken H. J. et al., 2012, *A&A*, 544, A156
- Mendel J. T. et al., 2015, *ApJ*, 804, L4
- Meurer G. R., Heckman T. M., Calzetti D., 1999, *ApJ*, 521, 64
- Muzzin A. et al., 2013, *ApJ*, 777, 18
- Noeske K. G., Weiner B. J., Faber S. M. e. a., 2007, *ApJ*, 660, L43
- Oke J. B., Gunn J. E., 1983, *ApJ*, 266, 713
- Onodera M. et al., 2014, *ArXiv e-prints*
- Pacifici C., Kassin S. A., Weiner B., Charlot S., Gardner J. P., 2013, *ApJ*, 762, L15
- Papovich C. et al., 2006, *ApJ*, 640, 92
- Pérez-González P. G., Cava A., et al. B., 2013, *ApJ*, 762, 46
- Pérez-González P. G., Gil de Paz A., Zamorano J., Gallego J., Alonso-Herrero A., Aragón-Salamanca A., 2003, *MNRAS*, 338, 508
- Pérez-González P. G. et al., 2005, *ApJ*, 630, 82
- Pérez-González P. G. et al., 2008, *ApJ*, 675, 234
- Pozzetti L. et al., 2010, *A&A*, 523, A13
- Prieto M., Eliche-Moral M. C., 2015, *MNRAS*, 451, 1158
- Prieto M. et al., 2013, *MNRAS*, 428, 999
- Renzini A., 2006, *ARA&A*, 44, 141
- Rodighiero G., Cimatti A., Gruppioni C., Popesso P., Andreani P. e. a., 2010, *A&A*, 518, L25
- Rujopakarn W., Rieke G. H., Weiner B. J., Pérez-González P., Rex M., Walth G. L., Kartaltepe J. S., 2013, *ApJ*, 767, 73
- Santini P. et al., 2015, *ApJ*, 801, 97
- Santini P. et al., 2009, *A&A*, 504, 751
- Saracco P. et al., 2005, *MNRAS*, 357, L40
- Schiavon R. P. et al., 2006, *ApJ*, 651, L93
- Shankar F. et al., 2015, *ApJ*, 802, 73
- Speagle J. S., Steinhardt C. L., Capak P. L., Silverman J. D., 2014, *ApJS*, 214, 15
- Spergel D. N. et al., 2003, *ApJS*, 148, 175
- Tacconi L. J. et al., 2010, *Nature*, 463, 781
- Takeuchi T. T., Yuan F.-T., Ikeyama A., Murata K. L., Inoue A. K., 2012, *ApJ*, 755, 144
- Thomas D., Maraston C., Bender R., Mendes de Oliveira C., 2005, *ApJ*, 621, 673
- Thomas D., Maraston C., Schawinski K., Sarzi M., Silk J., 2010, *MNRAS*, 404, 1775
- Tomczak A. R. et al., 2014, *ApJ*, 783, 85
- Tremonti C. A. et al., 2004, *ApJ*, 613, 898
- Trujillo I. et al., 2006, *ApJ*, 650, 18
- van Dokkum P. G. et al., 2011, *ApJ*, 743, L15
- van Dokkum P. G. et al., 2008, *ApJ*, 677, L5
- Whitaker K. E. et al., 2011, *ApJ*, 735, 86
- Whitaker K. E. et al., 2013, *ApJ*, 770, L39
- Worthey G., 1998, *PASP*, 110, 888
- Worthey G., Faber S. M., Gonzalez J. J., 1992, *ApJ*, 398, 69